Doctoral Thesis

The stoichiometry and function of the Kv4 channel complex vary depending on the relative expression level of each subunit

Masahiro Kitazawa

Department of Physiological Sciences, School of Life Science,

The Graduate University for Advanced Studies (SOKENDAI)

Contents

Abstract

Function of membrane proteins such as ion channels is often regulated by the accessary subunits. Therefore, the stoichiometry change can give rise to the wide variety of the biophysical properties of the complex and thus affect the cell excitability. Kv4, a member of voltage-gated K^+ channel family, is expressed in neurons and ventricular myocytes, and regulates the cell excitability. It is known that the function of Kv4 changes with various subunits in physiological condition. K^+ channel interacting protein (KChIP) and dipeptidyl aminopeptidase-like protein (DPP) are well-known auxiliary subunits for Kv4. KChIP increases the current amplitude of Kv4, decelerates the inactivation and accelerates the recovery from inactivation of Kv4. DPP is known to increase the current amplitude of Kv4 and accelerate the inactivation and the recovery from inactivation of Kv4.

The stoichiometries of Kv4/KChIP and Kv4/DPP complex have been partially revealed by the crystal structure analysis. However, it remains unknown whether the stoichiometries of Kv4/KChIP and Kv4/DPP complexes are fixed or variable. For DPP, even the number of DPPs binding to one Kv4 channel has not yet been determined. In this thesis, I addressed these questions using two methods; two-electrode voltage clamp (TEVC) and subunit counting by single-molecule imaging.

To examine how the expression level of KChIP affects the biophysical properties of Kv4, I expressed human Kv4.2 and rat KChIP4 in *Xenopus* oocytes with different

ratios and analyzed the currents under two-electrode voltage clamp. The recovery from inactivation of Kv4.2 was accelerated with the increase in the amount of co-expressed KChIP4. This raised the possibility that the binding number of KChIP4 could affect the properties of Kv4.2. To examine the effect of the number of KChIP4 on the biophysical properties of Kv4.2, I made two tandem repeat constructs (KChIP4-Kv4.2, KChIP4-Kv4.2-Kv4.2) in which the stoichiometry was strictly controlled. I expressed these constructs in *Xenopus* oocytes and analyzed the currents. Because Kv4.2 is a tetramer, KChIP4-Kv4.2 was expected to form a 4:4 channel (Kv4.2:KChIP4). Similarly, KChIP4-Kv4.2-Kv4.2 was expected to form a 4:2 channel. The 4:4 channel showed faster recovery from inactivation than the 4:2 channel, suggesting that the number of bound KChIP4 affects the biophysical property of Kv4.2. To directly examine whether the stoichiometry of Kv4.2/KChIP4 complex actually changes or not, the number of bound KChIP4 to a single Kv4.2 channel was evaluated using the subunit counting method by single-molecule imaging of monomeric enhanced GFP (mEGFP) fused to KChIP4. The number of bound KChIP4 was increased with the increase in the co-expressed KChIP4, indicating that the stoichiometry of Kv4.2/KChIP4 complex is not fixed but changes depending on the relative expression level of each subunit.

Next, I analyzed the stoichiometry of Kv4.2/DPP10 complex. As in the case of Kv4.2/KChIP4 complex, to examine whether the expression level of DPP10 can change

the biophysical properties of Kv4.2 or not, I injected human Kv4.2 and human DPP10 cRNA with different ratios and controlled the expression level of each subunit in *Xenopus* oocytes. The biophysical properties of Kv4.2 such as time-to-peak or the recovery from inactivation changed depending on the co-expression level of DPP10. Because the previous crystal structure analysis showed that DPP6 forms a dimer on the plasma membrane, I first analyzed the stoichiometry of DPP10 alone expressed in *Xenopus* oocytes. Approximately 70% of DPP10 on the membrane existed as dimers, whereas the rest existed as monomers. To determine the stoichiometry of Kv4.2/DPP10 complex, Kv4.2 and DPP10 were co-expressed with different ratios (100:1, 10:1, 1:1) and the stoichiometry was estimated using the subunit counting method. To confirm the co-assembly of Kv4.2 and DPP10, monomeric Cherry (mCherry) and mEGFP were tagged to Kv4.2 and DPP10, respectively. In the subunit counting experiments, two bleaching steps were mainly observed in all three ratios, suggesting that the stoichiometry of Kv4.2/DPP10 complex is flexible, but has a tendency to form the 4:2 channel complex.

Taken together, I conclude that the stoichiometry of Kv4.2/KChIP4 complex changes with no preferred stoichiometry while that of Kv4.2/DPP10 complex has a clear preference to 4:2, and that the stoichiometry of both Kv4.2/KChIP4 and Kv4.2/DPP10 complex changes depending on the relative expression level. As the stoichiometry difference affects the biophysical properties of Kv4.2, the stoichiometry

change of the Kv4.2 complex is thought to have a significant impact on the physiological function such as cardiac excitability.

Introduction

Membrane proteins, including ion channels, often function with various auxiliary subunits in physiological conditions. The stoichiometry of the complex determines the channel properties and therefore may affect the cell excitability. Kv4 is a member of the voltage gated K^+ (Kv) channel family. In common with other Kv channels, Kv4 α subunit has six transmembrane segments (S1-S6). The S1-S4 form a voltage-sensing domain (VSD) and, in particular, S4 segment is known to include several positively-charged amino acids (mainly arginine, R) and plays an important role in voltage sensing (Liman *et al.*, 1991; Bezanilla, 2000; Tombola *et al.*, 2006). The S5, P-loop and S6 form a pore domain. P-loop locating between S5 and S6 includes the selectivity filter containing a well-known signature sequence "GYG". Kv4 has the N and C-termini in intracellular side with "T1 domain" for assembly in the N-terminus. The hydrophilic residues in the T1 domain is known to contribute to Kv4 tetramerization (Li *et al.*, 1992; Shen *et al.*, 1993; Kreusch *et al.*, 1998).

Kv4 channel sub-family is comprised of three distinct genes: Kv4.1, Kv4.2 and Kv4.3. The transmembrane domains of Kv4 family are highly conserved while the N- and C- termini are relatively divergent. Kv4.1, 4.2 and 4.3 are mainly expressed in the brain and heart (Serodio *et al.*, 1994; Dixon *et al.*, 1996; Serodio & Rudy, 1998; An *et al.*, 2000; Nerbonne, 2000; Sanguinetti, 2002). According to the previous studies, Kv4.1 is expressed in brain at low levels while Kv4.2 and Kv4.3 are abundantly

expressed (Serodio *et al.*, 1996; Serodio & Rudy, 1998; Hattori *et al.*, 2003). Expression of Kv4.2 is predominant in the caudate putamen, the pontine nucleus and the medullary nuclei, whereas Kv4.3 is expressed in the substantia nigra pars compacta and the amygdara (Serodio & Rudy, 1998). In neurons, Kv4.2 is especially expressed in dendrites and produces the somatodendritic subthreshold A-type current (I_{SA}). I_{SA} is known to be involved in the control of repetitive firing and the attenuation of the back-propagation of action potentials (Serodio *et al.*, 1994; Chen *et al.*, 2006). In ventricular cardiac myocytes, Kv4.2 and Kv4.3 are mainly expressed and they are known to be expressed in epicardial myocytes than in endocardial ones (Dixon & McKinnon, 1994; Brahmajothi *et al.*, 1999). Kv4 generates the transient outward K^+ current (I_{to}) and shapes the first phase of repolarization in ventricular myocytes (Xu *et al.*, 1999; Nerbonne & Kass, 2005; Niwa & Nerbonne, 2010).

Kv4 forms the multimolecular complex with various subunits in physiological condition. K^+ channel interacting protein (KChIP) is one of the auxiliary subunits for Kv4. KChIP family was first identified by yeast two-hybrid screens using the N-terminus of Kv4 α subunit (An *et al.*, 2000). Members of the KChIP family consist of KChIP1-4, with a large number of alternatively spliced isoforms (Patel *et al.*, 2002a; Takimoto *et al.*, 2002; Burgoyne, 2007; Norris *et al.*, 2010). KChIP3 is also known as calsenilin (Buxbaum *et al.*, 1998), and as DREAM (downstream regulatory element antagonistic modulator) (Carrion *et al.*, 1999). KChIPs are the cytoplasmic protein

and have a conserved C-terminal core domain (Pongs & Schwarz, 2010). On the other hand, the N-termini of KChIPs are diverse not only in amino acid sequences but also in length (An *et al.*, 2000; Jerng *et al.*, 2004a; Burgoyne, 2007; Pongs & Schwarz, 2010). KChIP is known to possess four EF hands (EF1-4) for calcium binding. EF2, 3 and 4 mainly contribute to the Ca^{2+} binding (An *et al.*, 2000). KChIPs have substantial effects on the various properties of Kv4. First, KChIP promotes the surface expression of Kv4 and increases the current amplitude of Kv4 (Shibata *et al.*, 2003; Hasdemir *et al.*, 2005). Second, KChIP binding slows the inactivation of Kv4 by restricting the movement of the N-terminus, which may occlude the ion channel pore (Gebauer *et al.*, 2004). Third, KChIP accelerates the recovery from inactivation of Kv4 (Patel *et al.*, 2002b; Patel *et al.*, 2004; Hovind & Campbell, 2011). According to the crystal structure analysis of Kv4.3/KChIP1 complex, Kv4.3 interacts with KChIP at two sites (Pioletti *et al.*, 2006; Wang *et al.*, 2007). Site 1 is comprised of the area between 3rd and 21st amino acid residues of a conserved hydrophobic segment in the N-terminal side of T1 domain of Kv4.3 and a large hydrophobic pocket which is formed by KChIP1. Site 2 is between the H2 helix of KChIP1 and the T1 domain of Kv4.3. KChIP1 interacts at site 1 with one Kv4.3 subunit and at site 2 with another adjacent subunit. This crystallography analysis also demonstrates that four Kv4.3 α subunits and four KChIP1subunits form the octameric structure (Pioletti *et al.*, 2006; Wang *et al.*, 2007).

Although there are sufficient evidences showing that KChIP interacts with Kv4 channels and changes the properties, the Kv4 current in the presence of KChIPs was considerably different from the native current in neurons predominantly expressing Kv4 (Nadal *et al.*, 2003; Jerng *et al.*, 2005; Maffie & Rudy, 2008). This led to the hypothesis that Kv4 contains additional ancillary subunit(s). Another component of the Kv4 channel complex was then immunopurified and separated by SDS-PAGE. The new subunit was first identified as a 115 kDa protein. The protein was sequenced by tandem mass spectrometry and showed sequence similarity to dipeptidyl aminopeptidase protein (DPP) (Nadal *et al.*, 2003). DPPs belong to prolyl oligopeptidase family of serine protease family and contain well-known catalytic triad (Ser, His, Asp), however, this newly-identified protein (DPP6 or DPPX) lacks the catalytic serine (it is substituted to aspartic acid) and hence catalytic activity (Strop *et al.*, 2004; Maffie & Rudy, 2008; Jerng & Pfaffinger, 2014). The common topology of DPP family is the relatively short N terminus, one transmembrane and the huge extracellular C-terminus domains including a glycosylation domain, a cysteine-rich domain and an aminopeptidyl peptidase(-like) domain. DPP10 (or DPPY) is another non-catalytic type of DPP and the catalytic serine is substituted to glycine in DPP10 (Qi *et al.*, 2003). The members of DPP10 consist of four isoforms (DPP10a-d) (Jerng *et al.*, 2007; Pongs & Schwarz, 2010). All are known to bind to Kv4 α subunit and regulate its function including current amplitude. According to the previous

experiment, co-expression of Kv4.2 with DPP6 results in a ~9-fold increase in the channel protein on the plasma membrane (Foeger *et al.*, 2012). Additional KChIP co-expression further increases in the surface expression of Kv4 protein. This suggests that KChIP and DPP increase the current amplitude independently (Foeger *et al.*, 2012). As mentioned above, KChIP facilitates the trafficking of the Kv4 channel protein to the plasma membrane (Shibata *et al.*, 2003; Hasdemir *et al.*, 2005). On the other hand, DPP is thought to slow degradation of Kv4 by increasing retention on the plasma membrane (Foeger *et al.*, 2012). Although the mechanism remains unknown, DPP accelerates the inactivation and the recovery from inactivation of Kv4 (Jerng *et al.*, 2004b; Radicke *et al.*, 2005; Jerng *et al.*, 2007; Jerng *et al.*, 2009). The region from the N-terminus to the end of the transmembrane of DPP10 plays an important role in binding to the S1-S2 segments of the Kv4 for the complex formation (Ren *et al.*, 2005). It remains uncertain how many DPP molecules can bind to a tetrameric Kv4 channel. Although there is no available crystal structure for the Kv4/DPP complex, crystal structure of DPP6 alone has been determined and it was suggested that DPP6 exists as a dimer on the plasma membrane (Strop *et al.*, 2004). This implies a possibility that Kv4 and DPP may form the 4:2 or the 4:4 (Kv4:DPP) channel. A previous experiment using tandem repeat constructs suggests that Kv4.2 channel requires four DPP6 subunits to be fully modulated (Soh & Goldstein, 2008).

In the first part of this thesis, to examine how the expression level of KChIP4

affects the biophysical properties of Kv4.2, I tested various amounts of Kv4.2 and KChIP4 cRNAs and expressed both subunits with different ratios. The electrophysiological properties of Kv4.2 gradually changed along with the increase in the KChIP4 expression. Next, I made two tandem repeat constructs, in which the stoichiometry of Kv4.2 and KChIP4 was fixed, and observed that the speed of the recovery from inactivation of Kv4.2 were regulated by the number of KChIP4 subunits bound to Kv4.2. Finally, I determined the stoichiometry of Kv4.2/KChIP4 complex with the subunit counting method by single-molecule imaging. I found that the stoichiometry of Kv4.2/KChIP4 complex changed depending on the relative expression level of each subunit. In the second part, I examined the stoichiometry of Kv4.2/DPP10 complex. The electrophysiological experiments showed that the expression level of DPP10 also affected the biophysical properties of Kv4.2, as in the case of KChIP4. I examined the stoichiometry of Kv4.2/DPP10 complex and observed that the stoichiometry of Kv4.2/DPP10 complex had a preference to the 4:2 stoichiometry, showing a clear contrast to the Kv4.2/KChIP4 case without any clear preferred stoichiometry.

Materials and Methods

Molecular Biology

Human Kv4.2 (NM_012281.2), rat KChIP4 (NM_181365.2) and human DPP10 (AK_296490.1) were subcloned into the pGEMHE expression vector. To make the KChIP4-Kv4.2 construct, a flexible GGS linker (GGSGGSGGSGGSGG) and the NotI site were introduced to the N-terminus of Kv4.2 by PCR using KOD plus Ver.2 (Toyobo) ("NotI-linker-Kv4.2"). NotI site was also introduced to the C-terminus of KChIP4 by PCR ("KChIP4-NotI"). NotI-linker-Kv4.2 and KChIP4-NotI were fused and inserted into pGEMHE expression vector. To make the KChIP4-Kv4.2-Kv4.2 tandem construct, we first made Kv4.2-Kv4.2 construct by PCR. A flexible GGS linker and EcoRI site were introduced to the C-terminus of Kv4.2 ("Kv4.2-linker-EcoRI"). EcoRI site was also introduced to another Kv4.2 and the fragments cut by EcoRI site were fused. The fragment from Kv4.2-Kv4.2 cut by unique BamHI site in Kv4.2 was inserted into the BamHI site of the KChIP4-Kv4.2 tandem construct. For the monomeric enhanced green fluorescent protein (mEGFP)-tagged constructs, mEGFP was fused to the C-terminus of Kv4.2 or KChIP4 and the N-terminus of DPP10 with a flexible GGS linker (Kv4.2-mEGFP, KChIP4-mEGFP and mEGFP-DPP10). To make the monomeric Cherry (mCherry)-tagged Kv4.2, mCherry was fused to the C-terminus of Kv4.2 with a flexible GGS linker (Kv4.2-mCherry). For Kv4.2-KChIP4-mEGFP, we first made

Kv4.2-KChIP4 construct, in which Kv4.2-linker-EcoRI was fused to KChIP4 containing EcoRI in the N-terminus. The fragment from KChIP4-mEGFP cut by unique EcoT22I site in KChIP4 and HindIII site in the vector was inserted between EcoT22I and HindIII sites in Kv4.2-KChIP4 construct. All constructs were confirmed by DNA sequencing. cRNA was then synthesized from the linearized plasmid cDNA using T7 mMessage mMachine kit (Ambion).

Two-Electrode Voltage Clamp with *Xenopus laevis* oocytes

Oocytes were collected from *Xenopus laevis* anesthetized in water containing 0.15% tricaine, and treated with collagenase (2 mg/ml; type 1; Sigma-Aldrich) for 6-7 hrs to remove the follicular cell layer. Oocytes of similar size at stage V or VI were injected with 50 nl of cRNA solution. The injected oocytes were incubated for 1-3 days at 17°C in frog ringer solution containing (in mM): 88 NaCl, 1 KCl, 2.4 $NaHCO_3$, 0.3 $Ca(NO_3)_2$, 0.41 $CaCl_2$, and 0.82 $MgSO_4$, pH 7.6, with 0.1% penicillin-streptomaycin solution (Sigma-Aldrich). All experiments were approved by the Animal Care Committee of the National Institute for Physiological Sciences, and performed following the institutional guideline. On 1-3 days after cRNA injection, K^+ currents were recorded under two-electrode voltage clamp using OC-725C amplifier (Warner Instruments). All experiments were performed at room temperature. The microelectrodes were drawn from borosilicate glass capillaries (World Precision

Instruments) to a resistance of 0.2-0.5 MΩ and filled with 3 M K-acetate and 10 mM KCl (pH 7.2). ND-96 was used for the bath solution containing (in mM): 96 NaCl, 2 KCl, 1.8 $CaCl_2$, 1 $MgCl_2$ and 5 HEPES, pH 7.2. Holding potential was at -80 mV or 100mV. Stimulation, data acquisition and data analysis were performed using Digidata 1440 and pCLAMP 10.3 software (Molecular Devices). Data from the amplifier were digitized at 10 kHz and filtered at 1 kHz.

Western Blotting

One day after injection, oocytes were sonicated in PBS containing (in mM): 137 NaCl, 2.7 KCl, 10 Na_2HPO_4, 1.76 KH_2PO_4, with protein inhibitor (Complete, Mini, EDTA-free, Roche Applied Science). To remove the yolk, the homogenates were centrifuged at 3000 rpm, 4°C for 10 min and the supernatant were collected as protein extract from oocytes. The protein extracts were treated with SDS-DTT solution containing (in mM): 50 Tris-HCl (pH=6.8), 100 DTT, 10% Glycerol, 0.1% Bromophenol blue (BPB), 2% SDS, and boiled at 100°C for 5 min. SDS-PAGE was performed using 2-15% gradient gel in SDS-PAGE buffer containing (in mM): 25 Tris-base, 192 Glycine, 0.1% SDS. Protein concentration for each sample was measured by Bradford protein assay (Bradford, 1976). The amount of each loaded protein was adjusted to 10 μg. The proteins were transferred to polyvinylidene fluoride (PVDF) membranes in western buffer containing (in mM): 25 Tris-base, 192

Glycine. The membranes with bound protein were treated with 5 % skim milk in TBST solution containing (in mM): 20 Tris-HCl (pH=8.0), 150 NaCl, 0.05% Tween 20. Membranes were then incubated with primary antibodies (1:250) at 37°C for 1hr. The primary antibodies against KChIP4 used in this study were Anti-KCNIP4 (HPA022862, Sigma-Aldrich). Bound primary antibodies were detected with HRP labeled donkey anti-rabbit IgG (1:1000) (GE Healthcare). Immunoreactivity was visualized using an enhanced chemiluminescence (ECL) detection kit (GE Healthcare) and was detected using a LAS-3000 image analyzer (Fujifilm).

Single-molecule subunit counting

12-20 hrs after injection, to remove the extracellular matrix, the oocytes were treated by the enzyme mix solution (1 U/ml neuraminidase and 1 mg/ml hyaluronidase; Sigma-Aldrich) for 15 minutes at 17°C. The oocytes were put in the 2x frog ringer solution and osmotically shrunk. The vitelline cells were then manually removed with forceps. The oocytes were placed on the high refractive index coverslip (n=1.78). The objective lens (Olympus 100×, N.A. 1.65) was mounted on the inverted microscope (Olympus, IX71). ND-96 was used as extracellular solution. mEGFP was excited with a Cyan 488-nm solid state laser (Spectra-Physics). mCherry was excited with an Orange 588-nm solid state laser (Coherent). iXon3 EMCCD camera (Andor) was used for the detection of the fluorescence spots. Sampling area was 25.6 × 25.6-μm^2 and

movies of 400 frames were acquired at 20 Hz for 20 s. Fluorescent intensity of each spot was measured from the off-line movie. Only the spots which were not overlapped with neighbor spots and stable (not moving) during the 20-s recording were used for data collection and analyses.

Data analysis

The ionic currents were analyzed using pCLAMP 10.3 (Molecular Devices) and Igor Pro software (WaveMetrics, inc). All current traces were analyzed without leak subtraction. To compare the speed of inactivation among each group, the currents were fitted by a single or double exponential function:

$$I = \sum_{i=1}^{n} A_i e^{-t/\tau i} + C$$

Where A_i is the amplitude(s) of each component, t is time, τ is the time constant(s), n is the number of component (1 or 2) and C is the non-inactivating component.

The kinetics of the recovery from inactivation was fitted with a single exponential function:

$$I = I_{peak}\,(1 - e^{-t/\tau\,rec})$$

Where I_{peak} is the current amplitude of complete recovery and τ_{rec} is the recovery time constant at -80 or -100 mV. I is normalized by the average of peak current amplitudes at first test pulse.

The steady state inactivation curves were fitted with a two-state Boltzmann

equation and the half inactivation voltage $V_{1/2}$was deduced.

$$I = I_{min} + \frac{I_{max} - I_{min}}{1 + e^{\frac{ZF}{RT}(V - V_{1/2})}}$$

Where I_{max} and I_{min} are the maximum and minimum current amplitude at test pulse, $V_{1/2}$ is the half inactivation voltage, Z is the effective charge, F is Faraday's constant, R is the gas constant, and T is the absolute temperature. For normalization, I was divided by I_{max}.

The distributions of subunit counting data were analyzed by Igor Pro software. For estimating the stoichiometry of the Kv4 channel subunits and the fluorescence probability for mEGFP, the distributions of observed bleaching steps were fitted with a binomial distribution $P(X = a)$,

$$P(X = a) = A\ {}_nC_a\ p^a (1-p)^{n-a}$$

Where A is the total number of spots, n is the number of bound subunits, a is the observed bleaching steps and p is the fluorescence probability of mEGFP.

Statistical Analyses

All data are presented as the mean ± S.E.M and n stands for the number of samples. Statistical differences were evaluated using Student's unpaired *t* test or Dunnett's test. Values of $P < 0.05$ were considered significant. *** stands for the

value of $P < 0.001$.

Results

KChIP4 and DPP10 modulate Kv4.2 channel properties

It is known that the properties of Kv4 are changed by the co-expression of KChIP or DPP (Patel *et al.*, 2004; Jerng *et al.*, 2005; Radicke *et al.*, 2005). To examine how KChIP4 or DPP10 change the properties of Kv4.2, Kv4.2 was expressed with KChIP4 or DPP10 in *Xenopus* oocyte. Both of DPP10 and KChIP4 increased the current amplitude of Kv4.2 (Fig 1A). DPP10 accelerated the inactivation of Kv4.2. On the other hand, KChIP4 decelerated the inactivation of Kv4.2. When DPP10 and KChIP4 were co-expressed with Kv4.2 simultaneously, the inactivation speed was between Kv4.2 with DPP10 and Kv4.2 with KChIP4 (Fig 1A). The recovery from inactivation of Kv4.2 was accelerated when DPP10 or KChIP4 was expressed with Kv4.2 and the co-expression of the three subunits showed the fastest recovery from inactivation (Fig 1B).

Biophysical properties of Kv4.2 gradually change depending on the co-expression level of KChIP4

To examine the effect of expression level of KChIP4 in the modulation, I injected various amounts of KChIP4 cRNA (0, 0.05, 0.1, 0.25, 0.5, 1, 2.5, 5, 10 ng) with a constant amount of Kv4.2 cRNA (5 ng) in *Xenopus* oocytes and compared the current (Fig. 2A). To confirm that the KChIP4 protein level was properly controlled, I

checked the expression level of KChIP4 by western blotting. Two bands were observed with more than 0.5 ng of KChIP4 cRNA injection. The larger bands gradually intensified along with the increase in the injected amount of KChIP4 cRNA, indicating that the co-expression levels of KChIP4 were controlled as expected (Fig. 2B). KChIP is known to increase the current amplitude of Kv4 (An *et al.*, 2000; Bahring *et al.*, 2001; Hatano *et al.*, 2002). To examine whether or not the co-expression level of KChIP4 affects the biophysical properties of Kv4.2, various amounts of KChIP4 were expressed with Kv4.2. The current amplitudes of Kv4.2 gradually increased in the range between 0.25 ng and 2.5 ng of co-expressed KChIP4 (Fig. 2C). To examine the effect of KChIP4 on the surface expression of Kv4.2, Kv4.2-mEGFP was expressed with various amounts of KChIP4 cRNA (0, 0.005, 0.05 and 0.5 ng) in oocytes and the expression of Kv4.2 was evaluated by counting the number of fluorescent spots on the surface under TIRF microscopy (Fig. 3A). The expression of Kv4.2 was gradually augmented with the increase in the KChIP4 co-expression and showed considerable changes between 0.005 ng and 0.05 ng of co-injected KChIP4 cRNA (Fig. 3B).

Next I analyzed the biophysical properties of Kv4.2 with various amounts of KChIP4 expression. To examine whether or not the expression level of KChIP4 affects the activation of Kv4.2, I compared the I-V relationships of Kv4.2 with various amounts of KChIP4 and observed that normalized I-V relationships were not changed

by the amount of KChIP4 (Fig. 4A). In contrast, the steady-state inactivation showed a gradual positive shift by increasing co-expressed KChIP4. The amount of change is approximately +10 mV between Kv4.2 alone (-66.7 ± 2.2 mV; n = 3) and Kv4.2 (5 ng) + KChIP4 (10 ng) (-56.0 ± 1.3 mV; n = 5) in $V_{1/2}$ values of inactivation (Fig. 4B). The inactivation of Kv4.2 was also gradually decelerated with the increase in KChIP4. When the amount of co-expressed KChIP4 was between 0 – 1 ng, the inactivation curves at each potential were best fitted by double exponential function with the fast and slow components (Fig. 4C). In all cases (0, 0.05, 0.1, 0.25, 0.5, 1 ng of co-expressed KChIP4), the fast components were dominant (Fig. 4D). The fast time constants of inactivation at +50 mV varied between 17.9 ± 0.6 ms (Kv4.2 alone; n = 3) and 37.3 ± 0.7 ms (Kv4.2 (5ng) + KChIP4 (1 ng); n = 5). On the other hand, when more than 2.5 ng of KChIP4 was co-expressed with Kv4.2, the inactivation curve of Kv4.2 was best fitted with a single exponential function. The time constants at +50 mV for 2.5, 5 and 10 ng of KChIP4 were 69.4 ± 2.3 ms (n = 8), 72.0 ± 2.3 ms (n = 7) and 69.7 ± 1.5 (n = 13), respectively. In each case, the time constant was gradually increased along with the increase in the membrane potential (Fig. 4C, D).

Next, I investigated how various amounts of KChIP4 modified the recovery from inactivation. The same range of KChIP4 cRNA as used in Figs.2 and 4 (0, 0.05, 0.1, 0.25, 0.5, 1, 2.5, 5, 10 ng) was co-injected with Kv4.2 cRNA (5 ng) and the currents were evoked by a two pulse protocol (Fig. 5A). Time courses of the recovery from

inactivation were plotted in Fig. 5B. The recovery time constants were determined by fitting with a single exponential function to the recovery curve in Fig. 5B. The recovery from inactivation of Kv4.2 was gradually accelerated between 0 and 1 ng of co-expressed KChIP4. The time constant was reduced from 358 ± 72 ms (Kv4.2 alone, n = 3) to 50 ± 3 ms (Kv4.2 (5 ng) + KChIP4 (2.5 ng), n = 8) (Fig. 5C).

Taken together, these gradual changes of electrophysiological properties with various amounts of co-expressed KChIP4 suggest that the number of bound KChIP4 to Kv4.2 channel changes by the expression level of KChIP4 and affects the biophysical properties of Kv4.2.

The recovery from inactivation of Kv4.2 was regulated by the number of bound KChIP4

To examine the possibility that the biophysical properties of Kv4.2 are changed by the number of bound KChIP4, I made two tandem repeat constructs, in which the stoichiometry of Kv4.2 and KChIP4 is strictly controlled. KChIP4-Kv4.2-Kv4.2 construct was expected to form the 4:2 channel (Kv4.2:KChIP4) and KChIP4-Kv4.2 construct was expected to form the 4:4 channel (Fig. 6A). The current traces from each construct were shown in Fig. 6B. They are not significantly different in terms of the current amplitude at +40mV. The averaged peak current amplitudes of 4:2 channel and 4:4 channel were 6.9 ± 1.8 μA and 4.8 ± 0.8 μA, respectively (Fig. 6B). I also

compared the I-V relationships, the inactivation time constants, and the voltage dependence of the steady-state inactivation between the 4:2 and the 4:4 channels. The current amplitude and the normalized I-V relationships were not significantly different between the 4:2 and the 4:4 channel (Fig. 7A, B). The 4:2 channel showed slightly slower inactivation than the 4:4 channel (Fig. 7C). The $V_{1/2}$ of the steady-state inactivation was slightly but significantly ($P < 0.01$) different between the 4:2 (-60.6 ± 0.3 mV, n = 3) and the 4:4 channel (-57.9 ± 0.5 mV, n = 4) (Fig. 7D). On the other hand, the recovery from inactivation of the 4:4 channel showed faster inactivation than the 4:2 channel (Fig. 8A). The 4:4 channel showed the similar kinetics to that of Kv4.2 (5 ng) with KChIP4 (5 ng) and the 4:2 channel showed the similar kinetics to that of Kv4.2 (5 ng) with KChIP4 (0.5 ng) (Fig. 8B). Each time course was fitted with a single exponential function. The recovery time constants of the 4:4 channel (68.6 ± 1.5 ms, n = 4) and the 4:2 channel (105.8 ± 4.2, n = 4) were significantly different ($P < 0.001$).

I next examined whether or not additional KChIP4 could bind to the residual binding sites of the 4:2 channel and further accelerate the recovery from inactivation. KChIP4-Kv4.2-Kv4.2 tandem construct (5 ng) was expressed with additional wild-type KChIP4 (5 ng) to compare the recovery kinetics. The recovery from inactivation of the 4:2 channel with additional KChIP4 showed similar kinetics to that of the 4:4 channel (Fig. 8B). The time constant of the 4:2 channel with KChIP4 was also fitted

with a single exponential function and the time constant of the 4:2 channel with KChIP4 (61.8 ± 1.0 ms, n = 4) was significantly smaller than that of the 4:2 channel (105.8 ± 4.2, n = 4) ($P < 0.001$) (Fig. 8C). These results suggest that the kinetics of recovery from inactivation in Kv4.2 is dependent on the number of bound KChIP4.

Kv4.2 forms a tetramer

Before determining the stoichiometry of Kv4.2/KChIP4 complex, I confirmed tetramer formation of Kv4.2 on the membrane using subunit counting method by single-molecule imaging (Ulbrich & Isacoff, 2007). The C-terminus of Kv4.2 was tagged with mEGFP (Kv4.2-mEGFP) and expressed in *Xenopus* oocyte (Fig. 9A). First, I confirmed that the currents of Kv4.2-mEGFP evoked by step pulses showed similar kinetics to those of wild type Kv4.2 (Fig. 9A). Next, I expressed Kv4.2-mEGFP with low density to minimize the probability of two spots overlapping and observed discrete fluorescent spots on the membrane under TIRF microscope. The fluorescent spots from Kv4.2-mEGFP were observed as clear and immobile spots (Fig. 9B). I analyzed the fluorescence intensity change from each spot and counted the number of bleaching steps. Because the probability of mEGFP to be fluorescent is not 100% due to misfolding of the mEGFP or other reasons, three, two and one bleaching spots were observed even in Kv4.2 channels known to form a tetramer (Fig. 9C). I counted the bleaching steps from total 168 spots. The obtained distribution

was fitted with a binomial distribution with p = 76%, suggesting that the fluorescent probability of mEGFP tagged to Kv4.2 is 76% (Fig. 9D). I repeated the experiment with another data set (188 spots) and again obtained p = 76%.

The stoichiometry of Kv4.2/KChIP4 complex changes depending on the relative expression level of each subunit

To determine the stoichiometry of Kv4.2/KChIP4 complex, mEGFP was fused to the C-terminus of KChIP4 (KChIP4-mEGFP) (Fig. 10A). Before the subunit counting experiment, I confirmed that tagged mEGFP did not affect the functions of KChIP4. The current of Kv4.2 (5 ng) with KChIP4-mEGFP (5 ng) showed a similar slow inactivation to that of Kv4.2 with wild type KChIP4 (5 ng) (Fig. 10B). Kv4.2 and KChIP4-mEGFP were expressed with three different ratios (Kv4.2/KChIP4-mEGFP = 100 : 1 (0.5 ng : 0.005 ng), 10 : 1 (0.1 ng : 0.01 ng) and 1 : 1 (0.05 ng : 0.05 ng)) and the fluorescent spots from Kv4.2/KChIP4-mEGFP complex were detected under TIRF conditions (Fig. 10C). The bleaching steps from the fluorescent spots were counted to obtain the distribution histograms (Fig. 10D). In oocytes expressing Kv4.2 and KChIP4-mEGFP with 1 : 1 and 10 : 1 ratios, the three and four bleaching spots were mainly observed and the two and one bleaching spots were minor. On the other hand, in oocytes expressing Kv4.2 and KChIP4-mEGFP with 100 : 1 ratio, the two and one bleaching steps were frequently observed. The largest number of the bleaching steps

was four in any case, suggesting that up to four KChIP4s can bind to single Kv4.2 channel. The distributions from bleaching steps were fitted by a binomial distribution with an apparent fluorescence probability (*p'*), which should be a product of (fluorescent probability of mEGFP) × (association probability of KChIP4-mEGFP with Kv4.2). The values of *p'* were 24% (100 : 1), 63% (10 : 1) and 76% (1 : 1), respectively. I repeated the experiments with second data sets and obtained the values of *p'* = 26% (100 :1), 63% (10 : 1) and 76% (1 : 1) (Fig. 10E). To estimate the fluorescent probability of mEGFP tagged to KChIP4, I made a Kv4.2-KChIP4-mEGFP tandem construct, in which KChIP4-mEGFP was fused to the C-terminus of Kv4.2 (Fig. 11A). Kv4.2-KChIP4-mEGFP construct is expected to form a 4:4 channel (Kv4.2 : KChIP4-mEGFP). Therefore, association probability of the channel complex formed by Kv4.2-KChIP4-mEGFP construct is supposed to be 100%. This construct was expressed on the plasma membrane and the fluorescent spots were detected under TIRF illumination (Fig. 11B). I analyzed the fluorescent intensity from each spot and counted the bleaching steps. The obtained distributions of bleaching spots were fitted by a binomial distribution with 77% of fluorescent probability of mEGFP attached to KChIP4 (Fig. 11C). By dividing *p'* of Fig. 10E by the fluorescent probability of mEGFP attached to KChIP4 (77%), I calculated association probabilities of KChIP4 with Kv4.2. Calculated association probabilities of KChIP4 with Kv4.2 from first data set were 32% (100 : 1), 83% (10 : 1) and 99% (1 : 1), respectively (Fig. 11D). Taken

together, the stoichiometry of Kv4.2/KChIP4 complex is not fixed but variable and changes depending on the expression level of KChIP4.

The stoichiometry of Kv4.2/KChIP4 complex is not significantly changed with co-expression of DPP10.

DPP is also known to bind to Kv4 and modify the biophysical properties of Kv4. In neurons, Kv4 forms a ternary complex with KChIP and DPP (Jerng *et al.*, 2005). To examine the possibility that co-expression of DPP can change the stoichiometry of Kv4/KChIP complex, I expressed simultaneously Kv4.2, KChIP4-mEGFP and DPP10 and observed that DPP10 accelerates the inactivation of Kv4.2/KChIP4 complex (Fig. 12A, B). I next estimated the stoichiometry of Kv4.2/KChIP4 complex with subunit counting by single-molecule imaging. Expression level of each subunit was controlled by the amount of injected cRNA (Kv4.2 : KChIP4-mEGFP : DPP10 = 100 : 1 : 100 (0.5 ng : 0.005 ng : 0.5 ng) and 10 : 1 : 10 (0.1 ng : 0.01 ng : 0.1 ng)) (Fig. 12C). The observed distributions were fitted by a binomial distribution with an apparent fluorescence probability (*p'*). The values of *p'* were 27% (100 : 1 : 100) and 69% (10 : 1 : 10). By dividing *p'* by the fluorescent probability of mEGFP attached to KChIP4 (77%), association probabilities of KChIP4 with Kv4.2 in the presence of DPP were obtained. Association probabilities were 36% (100 : 1 : 100) and 90 % (10 : 1 : 10), respectively (Fig. 12D). Compared with the case in the absence of DPP10, association

probabilities of KChIP4 with Kv4.2 were not significantly changed, suggesting that co-expression of DPP10 does not markedly affect the stoichiometry of Kv4.2/KChIP4 complex.

The biophysical properties of Kv4.2 change depending on the expression level of DPP10

DPP10 is another Kv4 subunit, which is known to increase the current amplitude of Kv4.2 and accelerates the inactivation and the recovery from inactivation of Kv4.2 (Jerng *et al.*, 2004b; Zagha *et al.*, 2005; Nadal *et al.*, 2006). I first investigated if the biophysical properties of Kv4.2 were dependent on the expression level of DPP10 as in the case of KChIP4. Kv4.2 (2.5 ng) was expressed with various amounts of DPP10 (0, 0.025, 0.25 and 2.5 ng) and the currents were recorded under two electrode voltage clamp (Fig. 13A). The normalized I-V relationships were not significantly different among each group (Fig. 13C). On the other hand, the current amplitudes at +40 mV, the inactivation and the time-to-peak of Kv4.2 changed with various amounts of co-expressed DPP10 (Fig. 13B & 14). The current amplitudes at +40 mV increased between 0.25 (3.2 ± 0.4 μA, n = 19) and 2.5 ng (8.6 ± 1.2μA, n = 10) of co-expressed DPP10 (Fig. 13B). The inactivation was gradually accelerated with the increase in the DPP10 co-expression. The inactivation curves were fitted with a double exponential function and the fast component dominantly contributed to the inactivation (Fig. 14A,

B). $V_{1/2}$ of the steady-state inactivation showed a slight hyperpolarized shift between 0.25 ng (-72.6 ± 0.4 mV, n = 8) and 2.5 ng (-74.6 ± 0.3, n = 9) of co-injected DPP10 (Fig. 14C). The time-to-peak was gradually accelerated depending on the expression level of DPP10 (Fig. 14D). The kinetics of the recovery from inactivation were tested using a two-pulse protocol (Fig. 15). A +40 mV depolarizing pulse was applied and a second +40mV test pulse was subsequently applied after hyperpolarizing at -100mV for 10-490 ms to measure the recovery from inactivation (Fig. 15A). The kinetics of the recovery from inactivation was fitted with a single exponential function (Fig. 15B). The time constants were diminished from 145.9 ± 2.7 ms (Kv4.2 (2.5 ng) + DPP10 (0.025 ng); n = 7) to 69.3 ± 3.2 ms (Kv4.2 (2.5 ng) + DPP10 (2.5 ng); n = 8), suggesting that the recovery from inactivation of Kv4.2 also gradually accelerated when more than 0.025 ng of DPP10 cRNA was injected with Kv4.2 cRNA (Fig. 15C).

Taken together, the biophysical properties of Kv4.2 were changed depending on the expression level of DPP10, as in the case of KChIP4 with Kv4.2.

Approximately 70% of DPP10s on the membrane exist as dimers

DPP6 is also known as an accessory subunit for Kv4 (Kim *et al.*, 2008; Sun *et al.*, 2011; Jerng & Pfaffinger, 2012). Crystal structure analyses demonstrated that the extracellular domain of DPP6 forms a dimer (Strop *et al.*, 2004). To examine whether DPP10 also exists as a dimer on the membrane or not, I made mEGFP tagged DPP10

(DPP10-mEGFP), in which mEGFP was fused to the intracellular N-terminus of DPP10 (Fig. 16A). DPP10-mEGFP alone was expressed in *Xenopus* oocytes and the fluorescent spots were observed with TIRF microscopy (Fig. 16B). I counted the bleaching steps of a total 185 spots and the numbers of spots for each bleaching steps were plotted as a histogram (Fig. 16C, D). The spots showing two and one bleaching steps were mainly observed and the spots showing three or four steps were minor, suggesting that DPP10 on the membrane exist as the mixture of monomers and dimers (Fig. 16C, D). The probability of mEGFP to be fluorescent is around 70-80% as shown in other samples including Kv4.2-mEGFP and KChIP4-mEGFP (Ulbrich & Isacoff, 2007; Nakajo *et al.*, 2010; Kitazawa *et al.*, 2014). Therefore, I could estimate the proportion of monomers and dimers based on the distributions obtained from a binomial distribution, with an assumption of fluorescent probability p = 80%, for example (Fig. 16E). Approximately 70% of the spots on the membrane consist of DPP10 dimers and around 30% were DPP10 monomers if 76% of mEGFP were fluorescent (Fig. 16E, F).

The stoichiometry of Kv4.2/DPP10 complex has a preference to 4:2

To examine the stoichiometry of Kv4.2/DPP10 complex, DPP10-mEGFP was expressed with Kv4.2 tagged with a red fluorescent protein mCherry (Kv4.2-mCherry) (Fig. 17A). I first confirmed that Kv4.2-mCherry (2.5 ng) was functional.

Kv4.2-mCherry (2.5 ng) with DPP10-mEGFP (2.5 ng) showed fast inactivating currents similar to those of wild-type Kv4.2 (2.5 ng) with wild-type DPP10 (2.5 ng) (Fig. 17B). To confirm the co-assembly of Kv4.2-mCherry and DPP10-mEGFP, mCherry was first excited by a 588 nm laser and mEGFP was subsequently excited by a 488 nm laser (Fig. 17C, D, E).

Kv4.2-mCherry and DPP10-mEGFP were expressed in *Xenopus* oocytes with various cRNA ratios (100 : 1 (20 ng : 0.2 ng), 10 : 1 (20 ng : 2 ng), 1 : 1 (2ng : 2 ng)) and the bleaching steps from each mEGFP fluorescent spot were counted (Fig. 18A). Throughout the three different expression levels, the two bleaching step spots were always mainly observed although the three and four bleaching step spots were gradually increased depending on the increase in the DPP10 expression (Fig. 18B). This suggests that the stoichiometry of Kv4.2/DPP10 complex is variable depending on the expression level of DPP10, yet has a preference to form the 4:2 complex (Kv4.2 : DPP10).

Co-expression of KChIP4 does not significantly change the stoichiometry of Kv4.2/DPP10 complex

To test if the co-expression of KChIP4 affects the stoichiometry of Kv4.2/DPP10 complex, Kv4.2-mCherry, KChIP4 and DPP10-mEGFP were all expressed simultaneously (Fig. 19A). The stoichiometry of Kv4.2/DPP10 complex with various

amounts of cRNA ratios of Kv4.2, KChIP4 and DPP10 (Kv4.2-mCherry : KChIP4 : DPP10-mEGFP = 100 : 100 : 1 (5 ng : 5 ng : 0.05 ng), 10 : 10 : 1 (5 ng : 5 ng : 0.5 ng) and 1 : 1 : 1 (1 ng : 1 ng : 1ng)) were examined by the subunit counting. In all three cases, the two bleaching step spots were mainly observed and the three and four bleaching steps were increased along with the increase in the DPP10-mEGFP expression (Fig. 19B). Compared with the stoichiometry of Kv4.2/DPP10 complex in the absence of KChIP4 (Fig. 18B), no notable stoichiometry changes were observed in the presence of KChIP4, suggesting that the stoichiometry of Kv4.2/DPP10 complex was independent of KChIP4 expression, similarly to the stoichiometry of Kv4.2/KChIP4 which was independent of DPP10 expression (Fig. 12).

Discussions

In this doctoral thesis, I have analyzed the biophysical properties and stoichiometries of Kv4.2/KChIP4 and Kv4.2/DPP10 complex with various expression levels of each subunit. The biophysical properties of Kv4.2/KChIP4 and Kv4.2/DPP10 complex were gradually changed with the change in the relative expression level of each subunit. The stoichiometry of Kv4.2/KChIP4 complex was also gradually changed depending on the expression level of KChIP4 with no specific preference, whereas the stoichiometry of Kv4.2/DPP10 complex had a preference to 4:2 (Fig. 20).

The biophysical properties of Kv4 channel complex change depending on the subunit composition

Previous studies demonstrated that KChIP proteins including KChIP4 (not KChIP4a containing K^+ channel inactivation suppressor domain (Holmqvist *et al.*, 2002; Jerng & Pfaffinger, 2008; Liang *et al.*, 2009; Tang *et al.*, 2013)) increase the current amplitude, decelerate the inactivation and accelerate the recovery from inactivation of Kv4 (An *et al.*, 2000; Patel *et al.*, 2002b; Jerng *et al.*, 2005). DPP10 (and DPP6), another Kv4 subunit, is known to increase the current amplitude and accelerate the inactivation and the recovery from inactivation of Kv4 (Zagha *et al.*, 2005; Li *et al.*, 2006; Takimoto *et al.*, 2006). Consistent with these previous reports, I

observed that KChIP4 and DPP10 changed the biophysical properties of Kv4.2. I also found that the degree of current modulation was dependent on the amount of the co-injected cRNA (Figs. 2, 3, 4, 5, 13, 14 and 15). Interestingly, the current amplitude was increased with co-injection of more than 0.25 ng of KChIP4 cRNA (Fig. 2C), while the recovery from inactivation of Kv4.2 was already accelerated with even 0.05 ng of KChIP4 cRNA (Fig. 5C). In the case of DPP10, the current amplitude augmentation required 2.5 ng of DPP10 cRNA (Fig. 13B), whereas the recovery from inactivation of Kv4.2 was accelerated with 0.25 ng of DPP10 (Fig. 15C). These findings suggest that the number of subunits required for each modulation is different: the smaller number of KChIP4 or DPP10 subunit can accelerate the recovery from inactivation while more subunits are required for the augmentation of the current amplitude in both cases.

I observed that Kv4.2 tends to form 4:2 (Kv4.2 : DPP10) complex with DPP10 when the co-expression level of DPP10 is low and more DPP10 subunits can bind to Kv4.2 channel with the increase in the DPP10 co-expression (Fig. 18). According to the previous study using the tandem repeat constructs, the 4:4 (Kv4.2 : DPP6) channel and the 4:2 with additional DPP6 showed the biophysical properties similar to those of wild-type Kv4.2 with wild-type DPP6 ; therefore they concluded that Kv4.2 needs four DPP6 subunits to generate I_{SA} current (Soh & Goldstein, 2008). My observation does not support their conclusion that the binding of four DPP10 subunits requires for the

modulation of Kv4.2, but suggest that third and fourth DPP10 play a role in regulating the function of Kv4.2/DPP10 complex.

In the experiment using the tandem repeat constructs, I observed that the recovery from inactivation of the 4:4 channel (Kv4.2 : KChIP4) showed similar kinetics to that of Kv4.2 (5 ng) with KChIP4 (5 ng), and the 4:2 channel showed similar kinetics to that of Kv4.2 (5 ng) with KChIP4 (0.5 ng), respectively. The recovery from inactivation of the 4:2 channel with additional KChIP4 (5 ng) also showed similar kinetics to that of the 4:4 channel (Fig. 8B, C). This means that approximately two KChIP4 subunits bind to a single Kv4.2 channel with Kv4.2 (5 ng) and KChIP4 (0.5 ng) cRNAs, and also means that maximum four KChIP4 subunits can bind to a single Kv4.2 channel.

Unexpectedly, the 4:2 channel showed slower inactivation than the 4:4 channel (Fig. 7C). This result is not consistent with the result from wild-type Kv4.2 with wild-type KChIP4. According to the previous study, the N-terminus truncated mutant of Kv4.2 (Kv4.2Δ40) showed slower inactivation than that of wild-type Kv4.2, and the additional N-terminus peptide of Kv4.2 accelerated the inactivation of Kv4.2Δ40. Therefore, they concluded that the N-terminus of Kv4.2 generates the rapid inactivation by occluding the pore (Gebauer *et al.*, 2004). Because KChIP binding to the N-terminus of Kv4.2 decelerates the inactivation, free N-terminus without KChIP binding may be required for the rapid inactivation. In KChIP4-Kv4.2-Kv4.2 construct we made, the N-terminus of the second Kv4.2 is connected to the GGS linker. This

may restrict the movement of the N-terminus of the second Kv4.2 and cause the slower inactivation than the 4:4 channel.

The current amplitude of Kv4.2 was gradually increased depending on the co-expression level of KChIP4 (Fig. 2C). This suggests two possibilities: 1) KChIP4 increases the single channel conductance of Kv4.2. 2) The expression of Kv4.2 on the membrane was increased with the co-expression of KChIP4. Previous study revealed that KChIP does not affect the single channel conductance of Kv4.2 (~ 5 pS) (Beck *et al.*, 2002; Holmqvist *et al.*, 2002). It is also known that KChIP binding to the N-terminus of Kv4.2 can promote the Kv4.2 expression to the plasma membrane through endoplasmic reticulum (ER) or Golgi apparatus (Shibata *et al.*, 2003; Hasdemir *et al.*, 2005; Jerng & Pfaffinger, 2008; Foeger *et al.*, 2010). Consistent with these findings, I observed that the expression of Kv4.2 on the membrane is increased with co-expression of KChIP4 (Fig. 3). Taken together, the augmentation of the current amplitude of Kv4.2 is likely to be due to the increased surface expression of Kv4.2 by KChIP4 binding rather than the increase in the single channel conductance of Kv4.2.

Does the stoichiometry of Kv4.2 change on the membrane?

As mentioned above, KChIP promotes the surface expression of Kv4 from ER or Golgi (Shibata *et al.*, 2003; Hasdemir *et al.*, 2005; Jerng & Pfaffinger, 2008; Foeger *et al.*, 2010), suggesting that KChIP binds to Kv4.2 in ER or Golgi and is required for

transport of the complex to the plasma membrane. In addition, crystal structure showed that Kv4/KChIP complex forms the 4:4 channel (Pioletti *et al.*, 2006; Wang *et al.*, 2007). These data suggest that the Kv4.2-KChIP complex is formed in ER or Golgi and transported to the plasma membrane. On the other hand, I observed that the stoichiometry of Kv4.2/KChIP4 complex on the membrane changes depending on the relative expression level of each subunit. In addition to this, when KChIP4 alone (without Kv4.2) was expressed, freely moving KChIP4 proteins were observed in the cytosol. Therefore, free KChIP4 proteins in the cytosol could access and bind to the N-terminus of the Kv4.2 channel, and conversely bound KChIP4 could be released from the N-terminus of Kv4.2. My observations here suggest that the stoichiometry of Kv4.2/KChIP4 complex can be changed on the membrane depending on the expression level of KChIP4.

How is the Kv4.2/DPP10 complex formed?

Under the TIRF microscope, I found that approximately 70% of the DPP proteins on the membrane exist as dimers and the rest of approximately 30% exist as monomers (Fig. 16E, F). Which form of DPP10 binds to Kv4.2 and form the complex? In the previous study, the chimeras of Kv1.4 (not bind to DPP10) and Kv4.3, and the chimeras of DPP4 (not bind to Kv4.3) and DPP10 were constructed to identify the binding site between Kv4.3 and DPP10 (Ren *et al.*, 2005). The Kv4.3

chimera, which contains the N-terminus to the end of S1 segment (or the end of S2 segment) of Kv1.4, were unable to associate with DPP10. Also the DPP10 chimera containing the cytosolic and transmembrane domain of DPP4 was incapable of associating with Kv4.3. Crystal structure demonstrated that the extracellular domain of DPP6 forms a dimeric structure (Strop *et al.*, 2004). In addition to this finding, DPP4, which is a related protein but does not modulate Kv4, shows the catalytic activity when DPP4 forms a dimer (Chien *et al.*, 2004). The N-terminus and transmembrane domain are thought to bind to the S1 and S2 domain of Kv4. Because Kv4 forms a tetramer, there are four binding sites for DPPs in one Kv4.2 channel. If dimerized DPP10 are involved in the Kv4.2/DPP10 complex formation, four DPP10 dimers can bind to a single Kv4.2 channel. This means that maximum eight DPP10 subunits can exist in one Kv4.2/DPP10 complex (Fig. 21, left). However, single-molecule experiment demonstrated that up to four DPP10 subunits can bind to a single Kv4.2 channel (Fig. 18). These findings suggest that DPP10 subunit binds as a monomer and may form a dimeric structure in Kv4.2/DPP10 complex (Fig. 21, right).

Why does the stoichiometry of Kv4.2/DPP10 complex have a preference? The extracellular domain of the DPP family is quite large compared with the cytoplasmic and transmembrane domain (Jerng *et al.*, 2004b; Strop *et al.*, 2004; Jerng *et al.*, 2007). Because DPP itself has a preference to dimerization as shown in Fig. 16, one possibility is that two monomer DPP10 subunits form a dimer after binding to

Kv4.2 channel. The large extracellular domain might prevent the additional DPP10 from binding to Kv4.2.

The stoichiometry change in physiological condition

According to the previous studies, the expression levels of Kv4.2 and KChIP2 are oscillated along with the endogenous circadian rhythm and the expression ratio of Kv4.2 and KChIP2 changes in one day (Yamashita *et al.*, 2003; Jeyaraj *et al.*, 2012). The expression ratio difference affects the repolarizing duration of the action potential. This could cause ventricular arrhythmia and/or sudden death during a certain time of the day. In this study, I revealed that the stoichiometry of Kv4.2/KChIP4 complex changes depending on the expression level of KChIP4 and that the stoichiometry can affect the biophysical properties of Kv4.2 (Fig. 20A). The stoichiometry change I observed here may also be occurred in ventricular myocytes and have an impact on physiological functions such as heart rhythm.

References

An WF, Bowlby MR, Betty M, Cao J, Ling HP, Mendoza G, Hinson JW, Mattsson KI, Strassle BW, Trimmer JS & Rhodes KJ. (2000). Modulation of A-type potassium channels by a family of calcium sensors. *Nature* **403,** 553-556.

Bahring R, Dannenberg J, Peters HC, Leicher T, Pongs O & Isbrandt D. (2001). Conserved Kv4 N-terminal domain critical for effects of Kv channel-interacting protein 2.2 on channel expression and gating. *The Journal of biological chemistry* **276,** 23888-23894.

Beck EJ, Bowlby M, An WF, Rhodes KJ & Covarrubias M. (2002). Remodelling inactivation gating of Kv4 channels by KChIP1, a small-molecular-weight calcium-binding protein. *The Journal of physiology* **538,** 691-706.

Bezanilla F. (2000). The voltage sensor in voltage-dependent ion channels. *Physiological reviews* **80,** 555-592.

Bradford MM. (1976). A rapid and sensitive method for the quantitation of microgram quantities of protein utilizing the principle of protein-dye binding. *Analytical biochemistry* **72,** 248-254.

Brahmajothi MV, Campbell DL, Rasmusson RL, Morales MJ, Trimmer JS, Nerbonne JM & Strauss HC. (1999). Distinct transient outward potassium current (Ito) phenotypes and distribution of fast-inactivating potassium channel alpha subunits in ferret left ventricular myocytes. *The Journal of general physiology* **113,** 581-600.

Burgoyne RD. (2007). Neuronal calcium sensor proteins: generating diversity in neuronal Ca2+ signalling. *Nature reviews Neuroscience* **8,** 182-193.

Buxbaum JD, Choi EK, Luo Y, Lilliehook C, Crowley AC, Merriam DE & Wasco W. (1998). Calsenilin: a calcium-binding protein that interacts with the presenilins and regulates the levels of a presenilin fragment. *Nature medicine* **4,** 1177-1181.

Carrion AM, Link WA, Ledo F, Mellstrom B & Naranjo JR. (1999). DREAM is a Ca2+-regulated transcriptional repressor. *Nature* **398,** 80-84.

Chen X, Yuan LL, Zhao C, Birnbaum SG, Frick A, Jung WE, Schwarz TL, Sweatt JD & Johnston D. (2006). Deletion of Kv4.2 gene eliminates dendritic A-type K+ current and enhances induction of long-term potentiation in hippocampal CA1 pyramidal neurons. *The Journal of neuroscience : the official journal of the Society for Neuroscience* **26,** 12143-12151.

Chien CH, Huang LH, Chou CY, Chen YS, Han YS, Chang GG, Liang PH & Chen X. (2004). One site mutation disrupts dimer formation in human DPP-IV proteins. *The Journal of biological chemistry* **279,** 52338-52345.

Dixon JE & McKinnon D. (1994). Quantitative analysis of potassium channel mRNA expression in atrial and ventricular muscle of rats. *Circulation research* **75,** 252-260.

Dixon JE, Shi W, Wang HS, McDonald C, Yu H, Wymore RS, Cohen IS & McKinnon D. (1996). Role of the Kv4.3 K+ channel in ventricular muscle. A molecular correlate for the transient outward current. *Circulation research* **79,** 659-668.

Foeger NC, Marionneau C & Nerbonne JM. (2010). Co-assembly of Kv4 {alpha} subunits with K+ channel-interacting protein 2 stabilizes protein expression and promotes surface retention of channel complexes. *The Journal of biological chemistry* **285,** 33413-33422.

Foeger NC, Norris AJ, Wren LM & Nerbonne JM. (2012). Augmentation of Kv4.2-encoded currents by accessory dipeptidyl peptidase 6 and 10 subunits reflects selective cell surface Kv4.2 protein stabilization. *The Journal of biological chemistry* **287,** 9640-9650.

Gebauer M, Isbrandt D, Sauter K, Callsen B, Nolting A, Pongs O & Bahring R. (2004). N-type inactivation features of Kv4.2 channel gating. *Biophysical journal* **86,** 210-223.

Hasdemir B, Fitzgerald DJ, Prior IA, Tepikin AV & Burgoyne RD. (2005). Traffic of Kv4 K+ channels mediated by KChIP1 is via a novel post-ER vesicular pathway. *The Journal of cell biology* **171,** 459-469.

Hatano N, Ohya S & Imaizumi Y. (2002). Functional interaction between KChIP1 and GFP-fused Kv4.3L co-expressed in HEK293 cells. *Pflugers Archiv : European journal of physiology* **444,** 80-88.

Hattori S, Murakami F & Song WJ. (2003). Quantitative relationship between Kv4.2 mRNA and A-type K+ current in rat striatal cholinergic interneurons during development. *Journal of neurophysiology* **90,** 175-183.

Holmqvist MH, Cao J, Hernandez-Pineda R, Jacobson MD, Carroll KI, Sung MA, Betty M, Ge P, Gilbride KJ, Brown ME, Jurman ME, Lawson D, Silos-Santiago I, Xie Y, Covarrubias M, Rhodes KJ, Distefano PS & An WF. (2002). Elimination of fast inactivation in Kv4 A-type potassium channels by an auxiliary subunit domain. *Proceedings of the National Academy of Sciences of the United States of America* **99,** 1035-1040.

Hovind LJ & Campbell DL. (2011). The "structurally minimal" isoform KChIP2d modulates recovery of K(v)4.3 N-terminal deletion mutant Delta2-39. *Channels* **5,** 225-227.

Jerng HH, Dougherty K, Covarrubias M & Pfaffinger PJ. (2009). A novel N-terminal motif of dipeptidyl peptidase-like proteins produces rapid inactivation of KV4.2 channels by a pore-blocking mechanism. *Channels* **3,** 448-461.

Jerng HH, Kunjilwar K & Pfaffinger PJ. (2005). Multiprotein assembly of Kv4.2, KChIP3 and DPP10 produces ternary channel complexes with ISA-like properties. *The Journal of physiology* **568,** 767-788.

Jerng HH, Lauver AD & Pfaffinger PJ. (2007). DPP10 splice variants are localized in distinct neuronal populations and act to differentially regulate the inactivation properties of Kv4-based ion channels. *Molecular and cellular neurosciences* **35,** 604-624.

Jerng HH & Pfaffinger PJ. (2008). Multiple Kv channel-interacting proteins contain an N-terminal transmembrane domain that regulates Kv4 channel trafficking and gating. *The Journal of biological chemistry* **283,** 36046-36059.

Jerng HH & Pfaffinger PJ. (2012). Incorporation of DPP6a and DPP6K variants in ternary

Kv4 channel complex reconstitutes properties of A-type K current in rat cerebellar granule cells. *PloS one* **7,** e38205.

Jerng HH & Pfaffinger PJ. (2014). Modulatory mechanisms and multiple functions of somatodendritic A-type K (+) channel auxiliary subunits. *Frontiers in cellular neuroscience* **8,** 82.

Jerng HH, Pfaffinger PJ & Covarrubias M. (2004a). Molecular physiology and modulation of somatodendritic A-type potassium channels. *Molecular and cellular neurosciences* **27,** 343-369.

Jerng HH, Qian Y & Pfaffinger PJ. (2004b). Modulation of Kv4.2 channel expression and gating by dipeptidyl peptidase 10 (DPP10). *Biophysical journal* **87,** 2380-2396.

Jeyaraj D, Haldar SM, Wan X, McCauley MD, Ripperger JA, Hu K, Lu Y, Eapen BL, Sharma N, Ficker E, Cutler MJ, Gulick J, Sanbe A, Robbins J, Demolombe S, Kondratov RV, Shea SA, Albrecht U, Wehrens XH, Rosenbaum DS & Jain MK. (2012). Circadian rhythms govern cardiac repolarization and arrhythmogenesis. *Nature* **483,** 96-99.

Kim J, Nadal MS, Clemens AM, Baron M, Jung SC, Misumi Y, Rudy B & Hoffman DA. (2008). Kv4 accessory protein DPPX (DPP6) is a critical regulator of membrane excitability in hippocampal CA1 pyramidal neurons. *Journal of neurophysiology* **100,** 1835-1847.

Kitazawa M, Kubo Y & Nakajo K. (2014). The stoichiometry and biophysical properties of the Kv4 potassium channel complex with K+ channel-interacting protein (KChIP) subunits are variable, depending on the relative expression level. *The Journal of biological chemistry* **289,** 17597-17609.

Kreusch A, Pfaffinger PJ, Stevens CF & Choe S. (1998). Crystal structure of the tetramerization domain of the Shaker potassium channel. *Nature* **392,** 945-948.

Li HL, Qu YJ, Lu YC, Bondarenko VE, Wang S, Skerrett IM & Morales MJ. (2006). DPP10 is an inactivation modulatory protein of Kv4.3 and Kv1.4. *American journal of physiology Cell physiology* **291,** C966-976.

Li M, Jan YN & Jan LY. (1992). Specification of subunit assembly by the hydrophilic amino-terminal domain of the Shaker potassium channel. *Science* **257,** 1225-1230.

Liang P, Wang H, Chen H, Cui Y, Gu L, Chai J & Wang K. (2009). Structural Insights into KChIP4a Modulation of Kv4.3 Inactivation. *The Journal of biological chemistry* **284,** 4960-4967.

Liman ER, Hess P, Weaver F & Koren G. (1991). Voltage-sensing residues in the S4 region of a mammalian K+ channel. *Nature* **353,** 752-756.

Maffie J & Rudy B. (2008). Weighing the evidence for a ternary protein complex mediating A-type K+ currents in neurons. *The Journal of physiology* **586,** 5609-5623.

Nadal MS, Amarillo Y, Vega-Saenz de Miera E & Rudy B. (2006). Differential characterization of three alternative spliced isoforms of DPPX. *Brain research* **1094,** 1-12.

Nadal MS, Ozaita A, Amarillo Y, Vega-Saenz de Miera E, Ma Y, Mo W, Goldberg EM, Misumi Y, Ikehara Y, Neubert TA & Rudy B. (2003). The CD26-related dipeptidyl aminopeptidase-like protein DPPX is a critical component of neuronal A-type K+ channels. *Neuron* **37,** 449-461.

Nakajo K, Ulbrich MH, Kubo Y & Isacoff EY. (2010). Stoichiometry of the KCNQ1 - KCNE1 ion channel complex. *Proceedings of the National Academy of Sciences of the United States of America* **107,** 18862-18867.

Nerbonne JM. (2000). Molecular basis of functional voltage-gated K+ channel diversity in the mammalian myocardium. *The Journal of physiology* **525 Pt 2,** 285-298.

Nerbonne JM & Kass RS. (2005). Molecular physiology of cardiac repolarization. *Physiological reviews* **85,** 1205-1253.

Niwa N & Nerbonne JM. (2010). Molecular determinants of cardiac transient outward potassium current (I(to)) expression and regulation. *Journal of molecular and cellular cardiology* **48,** 12-25.

Norris AJ, Foeger NC & Nerbonne JM. (2010). Interdependent roles for accessory KChIP2, KChIP3, and KChIP4 subunits in the generation of Kv4-encoded IA channels in cortical pyramidal neurons. *The Journal of neuroscience : the official journal of the Society for Neuroscience* **30,** 13644-13655.

Patel SP, Campbell DL, Morales MJ & Strauss HC. (2002a). Heterogeneous expression of KChIP2 isoforms in the ferret heart. *The Journal of physiology* **539,** 649-656.

Patel SP, Campbell DL & Strauss HC. (2002b). Elucidating KChIP effects on Kv4.3 inactivation and recovery kinetics with a minimal KChIP2 isoform. *The Journal of physiology* **545,** 5-11.

Patel SP, Parai R, Parai R & Campbell DL. (2004). Regulation of Kv4.3 voltage-dependent gating kinetics by KChIP2 isoforms. *The Journal of physiology* **557,** 19-41.

Pioletti M, Findeisen F, Hura GL & Minor DL, Jr. (2006). Three-dimensional structure of the KChIP1-Kv4.3 T1 complex reveals a cross-shaped octamer. *Nature structural & molecular biology* **13,** 987-995.

Pongs O & Schwarz JR. (2010). Ancillary subunits associated with voltage-dependent K+ channels. *Physiological reviews* **90,** 755-796.

Qi SY, Riviere PJ, Trojnar J, Junien JL & Akinsanya KO. (2003). Cloning and characterization of dipeptidyl peptidase 10, a new member of an emerging subgroup of serine proteases. *The Biochemical journal* **373,** 179-189.

Radicke S, Cotella D, Graf EM, Ravens U & Wettwer E. (2005). Expression and function of dipeptidyl-aminopeptidase-like protein 6 as a putative beta-subunit of human cardiac transient outward current encoded by Kv4.3. *The Journal of physiology* **565,** 751-756.

Ren X, Hayashi Y, Yoshimura N & Takimoto K. (2005). Transmembrane interaction mediates complex formation between peptidase homologues and Kv4 channels. *Molecular and cellular neurosciences* **29,** 320-332.

Sanguinetti MC. (2002). Reduced transient outward K+ current and cardiac hypertrophy: causal relationship or epiphenomenon? *Circulation research* **90,** 497-499.

Serodio P, Kentros C & Rudy B. (1994). Identification of molecular components of A-type channels activating at subthreshold potentials. *Journal of neurophysiology* **72,** 1516-1529.

Serodio P & Rudy B. (1998). Differential expression of Kv4 K+ channel subunits mediating subthreshold transient K+ (A-type) currents in rat brain. *Journal of neurophysiology* **79,** 1081-1091.

Serodio P, Vega-Saenz de Miera E & Rudy B. (1996). Cloning of a novel component of A-type K+ channels operating at subthreshold potentials with unique expression in heart and brain. *Journal of neurophysiology* **75,** 2174-2179.

Shen NV, Chen X, Boyer MM & Pfaffinger PJ. (1993). Deletion analysis of K+ channel assembly. *Neuron* **11,** 67-76.

Shibata R, Misonou H, Campomanes CR, Anderson AE, Schrader LA, Doliveira LC, Carroll KI, Sweatt JD, Rhodes KJ & Trimmer JS. (2003). A fundamental role for KChIPs in determining the molecular properties and trafficking of Kv4.2 potassium channels. *The Journal of biological chemistry* **278,** 36445-36454.

Soh H & Goldstein SA. (2008). I SA channel complexes include four subunits each of DPP6 and Kv4.2. *The Journal of biological chemistry* **283,** 15072-15077.

Strop P, Bankovich AJ, Hansen KC, Garcia KC & Brunger AT. (2004). Structure of a human A-type potassium channel interacting protein DPPX, a member of the dipeptidyl aminopeptidase family. *Journal of molecular biology* **343,** 1055-1065.

Sun W, Maffie JK, Lin L, Petralia RS, Rudy B & Hoffman DA. (2011). DPP6 establishes the A-type K(+) current gradient critical for the regulation of dendritic excitability in CA1 hippocampal neurons. *Neuron* **71,** 1102-1115.

Takimoto K, Hayashi Y, Ren X & Yoshimura N. (2006). Species and tissue differences in the expression of DPPY splicing variants. *Biochemical and biophysical research*

communications **348,** 1094-1100.

Takimoto K, Yang EK & Conforti L. (2002). Palmitoylation of KChIP splicing variants is required for efficient cell surface expression of Kv4.3 channels. *The Journal of biological chemistry* **277,** 26904-26911.

Tang YQ, Liang P, Zhou J, Lu Y, Lei L, Bian X & Wang K. (2013). Auxiliary KChIP4a suppresses A-type K+ current through endoplasmic reticulum (ER) retention and promoting closed-state inactivation of Kv4 channels. *The Journal of biological chemistry* **288,** 14727-14741.

Tombola F, Pathak MM & Isacoff EY. (2006). How does voltage open an ion channel? *Annual review of cell and developmental biology* **22,** 23-52.

Ulbrich MH & Isacoff EY. (2007). Subunit counting in membrane-bound proteins. *Nature methods* **4,** 319-321.

Wang H, Yan Y, Liu Q, Huang Y, Shen Y, Chen L, Chen Y, Yang Q, Hao Q, Wang K & Chai J. (2007). Structural basis for modulation of Kv4 K+ channels by auxiliary KChIP subunits. *Nature neuroscience* **10,** 32-39.

Xu H, Li H & Nerbonne JM. (1999). Elimination of the transient outward current and action potential prolongation in mouse atrial myocytes expressing a dominant negative Kv4 alpha subunit. *The Journal of physiology* **519 Pt 1,** 11-21.

Yamashita T, Sekiguchi A, Iwasaki YK, Sagara K, Iinuma H, Hatano S, Fu LT & Watanabe H. (2003). Circadian variation of cardiac K+ channel gene expression. *Circulation* **107,** 1917-1922.

Zagha E, Ozaita A, Chang SY, Nadal MS, Lin U, Saganich MJ, McCormack T, Akinsanya KO, Qi SY & Rudy B. (2005). DPP10 modulates Kv4-mediated A-type potassium channels. *The Journal of biological chemistry* **280,** 18853-18861.

Figures and Legends

Figure 1

The biophysical properties of Kv4.2 are modulated by the auxiliary subunits.

(A) The representative current traces of Kv4.2, Kv4.2 with DPP10, Kv4.2 with KChIP4 and Kv4.2 with KChIP4 and DPP10 evoked by depolarizing step pulses. The holding potential was at -80 mV. After a 500-ms hyperpolarized at -110 mV to remove the inactivation, the currents were stimulated by the voltages for 1-s between -100 mV and +50 mV in 10 mV increments. (B) The recovery from inactivation of Kv4.2, Kv4.2 with DPP10, Kv4.2 with KChIP4 and Kv4.2 with KChIP4 and DPP10. The currents were elicited by two-pulse protocol. The holding potential was at -80 mV. After a +40 mV stimulation for 500 ms, the currents were hyperpolarized at -80 mV for each duration and were elicited by second +40 mV depolarization. The increments of the hyperpolarized duration were 40 ms for Kv4.2 and Kv4.2 with DPP10 and 20 ms for Kv4.2 with KChIP4 and Kv4.2 with KChIP4 and DPP10.

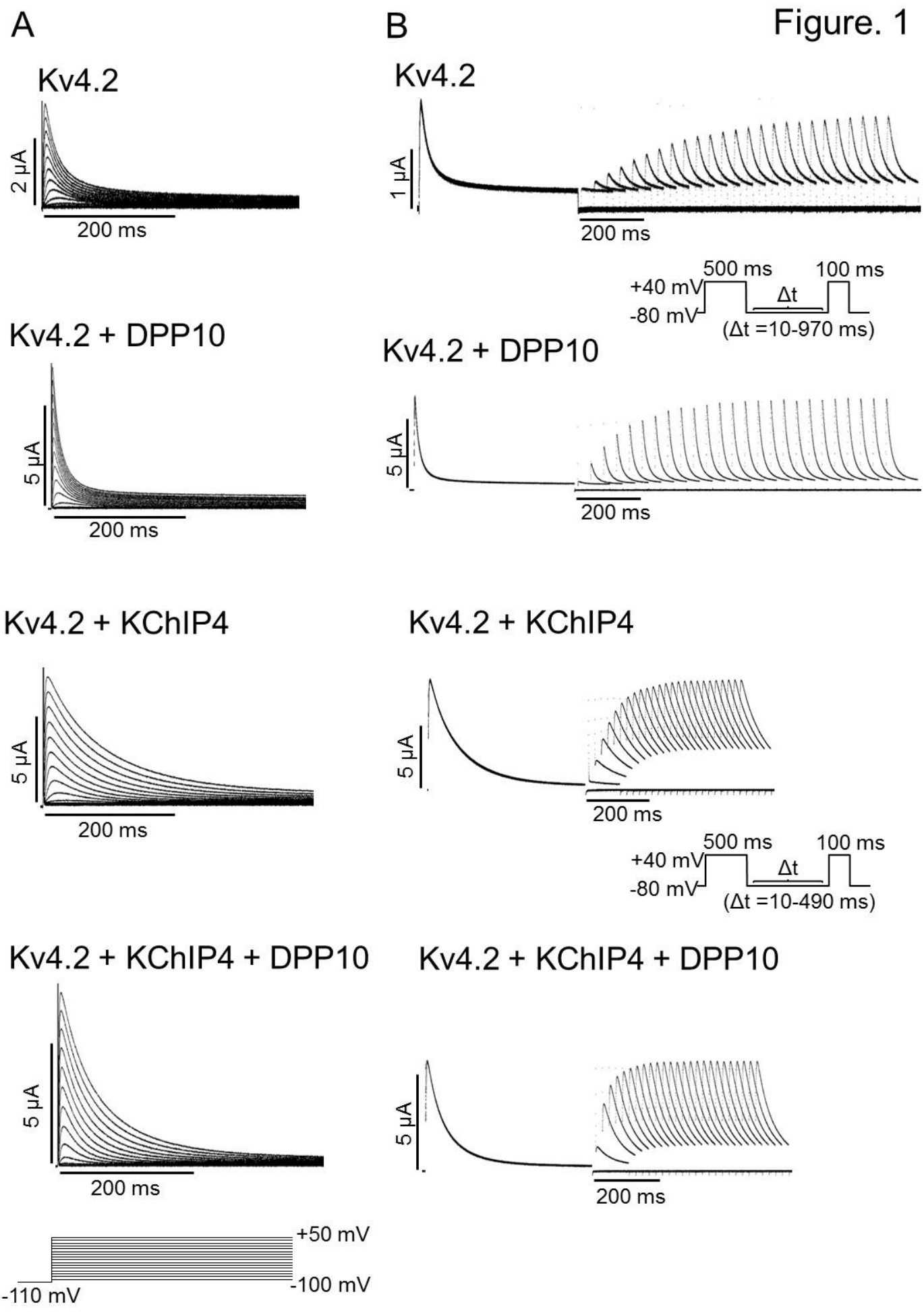
A
B
Figure. 1
Kv4.2
2 μA
200 ms
Kv4.2
1 μA
200 ms
500 ms
100 ms
+40 mV
Δt
-80 mV
(Δt =10-970 ms)
Kv4.2 + DPP10
5 μA
200 ms
Kv4.2 + DPP10
5 μA
200 ms
Kv4.2 + KChIP4
5 μA
200 ms
Kv4.2 + KChIP4
5 μA
200 ms
500 ms
100 ms
+40 mV
Δt
-80 mV
(Δt =10-490 ms)
Kv4.2 + KChIP4 + DPP10
5 μA
200 ms
+50 mV
-100 mV
-110 mV
Kv4.2 + KChIP4 + DPP10
5 μA
200 ms

Figure 2

Increase in the KChIP4 co-expression augments the current amplitude of Kv4.2.

(A) The representative current traces of Kv4.2 (5 ng), Kv4.2 (5 ng) with KChIP4 (0.05 ng), Kv4.2 (5 ng) with KChIP4 (0.5 ng) and Kv4.2 (5 ng) with KChIP4 (5 ng). The currents were evoked by step pulses shown below. (B) The co-expressed KChIP4 proteins with various amounts of injected cRNA were detected by western blotting. The expression of KChIP4 gradually increased with the increase in the amount of co-injected cRNA amount. (C) Comparison of the peak current amplitude of Kv4.2 with various amounts of KChIP4 cRNA (n = 6-12).

Figure. 2

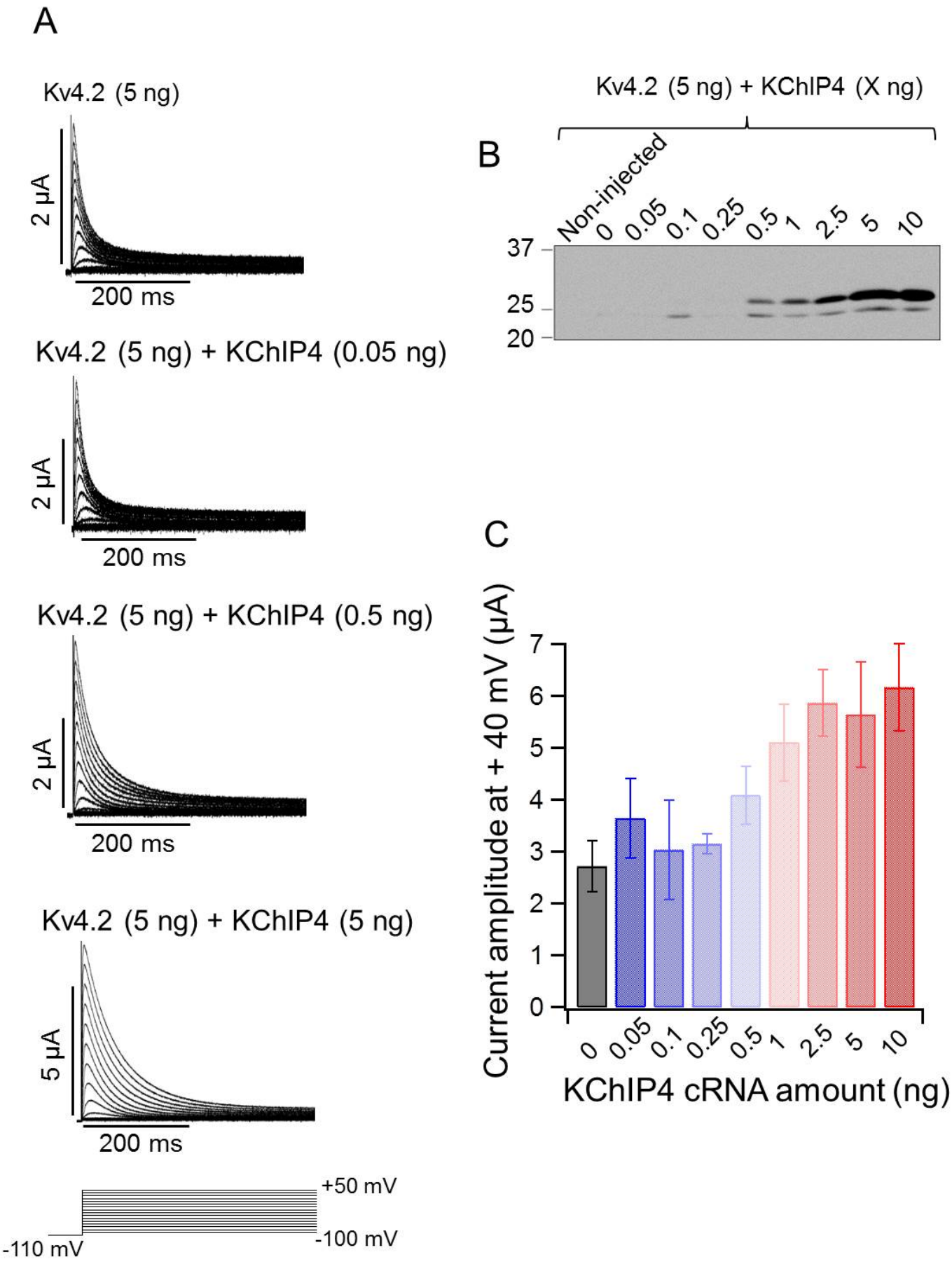
A
Kv4.2 (5 ng)
2 μA
200 ms
Kv4.2 (5 ng) + KChIP4 (0.05 ng)
2 μA
200 ms
Kv4.2 (5 ng) + KChIP4 (0.5 ng)
2 μA
200 ms
Kv4.2 (5 ng) + KChIP4 (5 ng)
5 μA
200 ms
+50 mV
-100 mV
-110 mV
B
Kv4.2 (5 ng) + KChIP4 (X ng)
Non-injected
0
0.05
0.1
0.25
0.5
1
2.5
5
10
37
25
20
C
Current amplitude at + 40 mV (μA)
0
1
2
3
4
5
6
7
0
0.05
0.1
0.25
0.5
1
2.5
5
10
KChIP4 cRNA amount (ng)

Figure 3

The expression of Kv4.2 is augmented with increase in the co-expressed KChIP4.

(A) The expressions of Kv4.2-mEGFP cRNA (0.05 ng) with various amounts of KChIP4 cRNA (0, 0.005, 0.05, 0.5 ng) were detected by the single molecule imaging under TIRF microscope. Each single spot corresponds to a tetrameric Kv4.2. White bars indicate 2 μm. (B) Comparison of the numbers of the fluorescent spots from Kv4.2-mEGFP with various amounts of co-injected KChIP4 cRNA (n = 10 for each).

Figure. 3

A

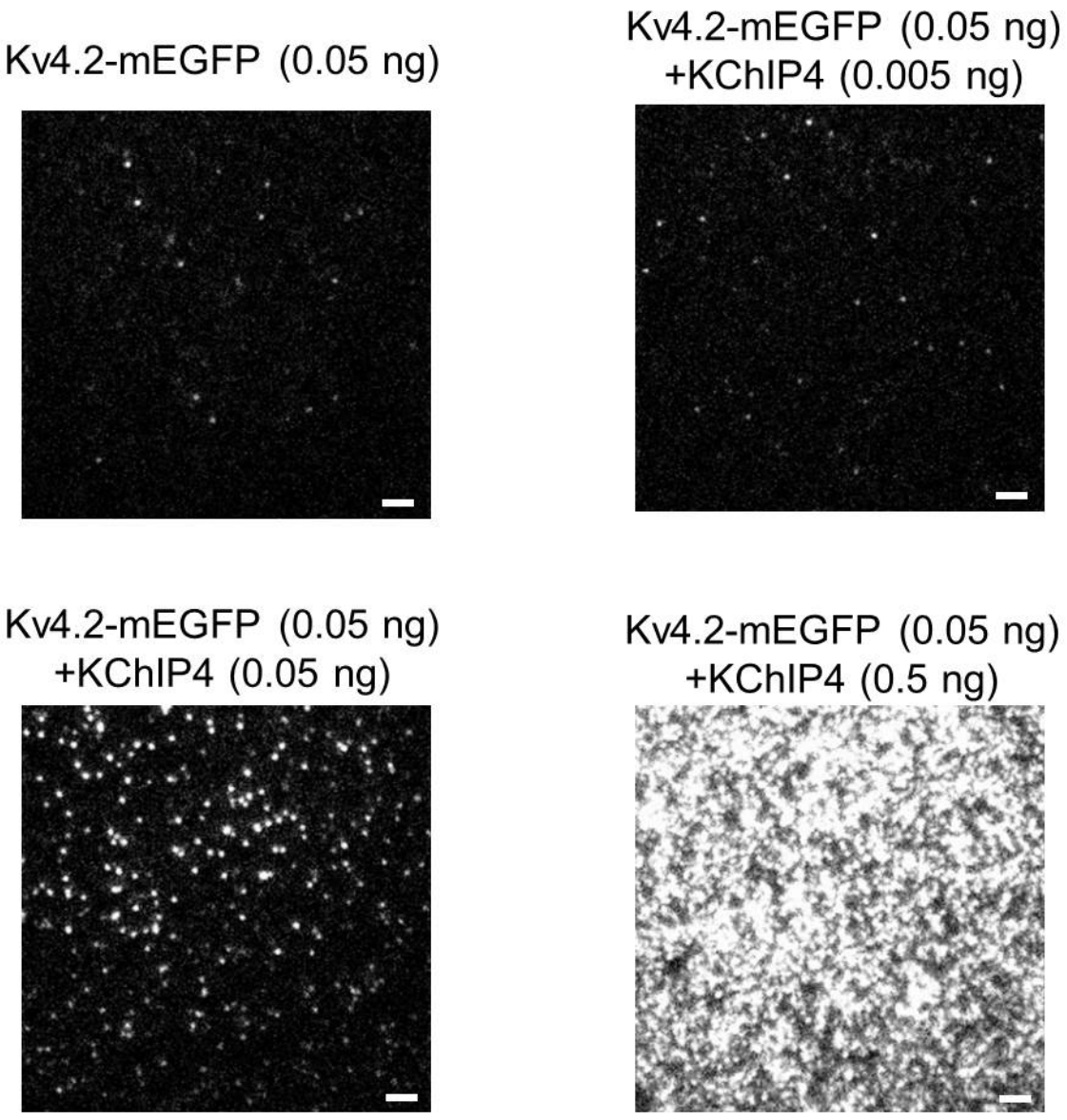
Kv4.2-mEGFP (0.05 ng)
Kv4.2-mEGFP (0.05 ng)
+KChIP4 (0.005 ng)
Kv4.2-mEGFP (0.05 ng)
+KChIP4 (0.05 ng)
Kv4.2-mEGFP (0.05 ng)
+KChIP4 (0.5 ng)

B

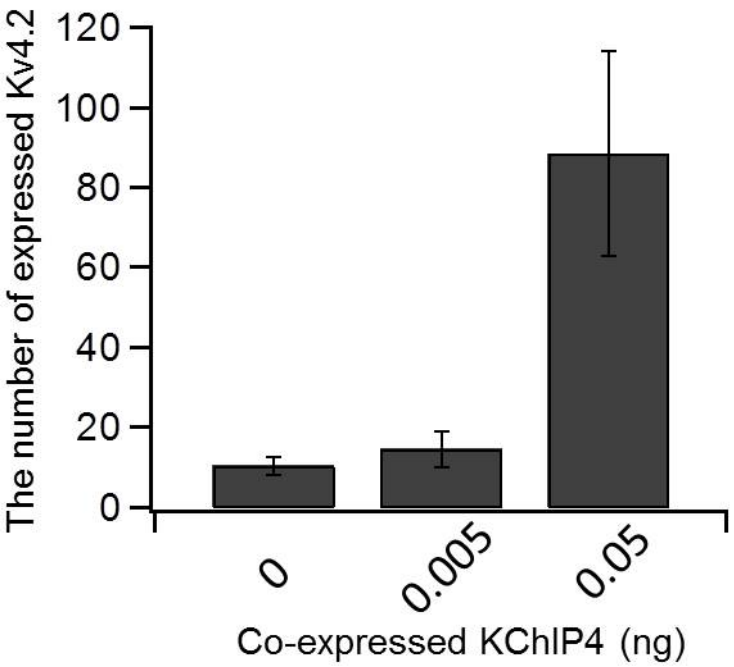
The number of expressed Kv4.2
120
100
80
60
40
20
0
0
0.005
0.05
Co-expressed KChIP4 (ng)

Figure 4

The biophysical properties of Kv4.2 are gradually affected with increase in the co-expressed KChIP4.

(A) I-V relationships of Kv4.2 (5 ng) with various amounts of KChIP4 cRNA (0-10 ng). The peak currents at each potential were normalized by the peak current amplitude at +50 mV and plotted (n = 3-13). (B) The steady-state inactivation curves of Kv4.2 with various amounts of KChIP4. After a 5-s pre-pulse at the voltage from -120 mV to 0 mV in 10 mV increment, the currents were stimulated by a test pulse at +40 mV (n = 3-5). (C) Comparison of the inactivation time constant of Kv4.2 with various amounts of co-expressed KChIP4. The inactivating current traces from Kv4.2 (5 ng) with KChIP4 (2.5, 5, 10 ng) were fitted with a single exponential function. On the other hand, the current traces from Kv4.2 (5 ng) with KChIP4 (0-1 ng) were fitted with a double exponential function (n = 3-13). (D) Fractional contributions of fast and slow time constants for Kv4.2 (5 ng) with KChIP4 (0-1 ng) were shown. Error bars show S.E.

Figure. 4

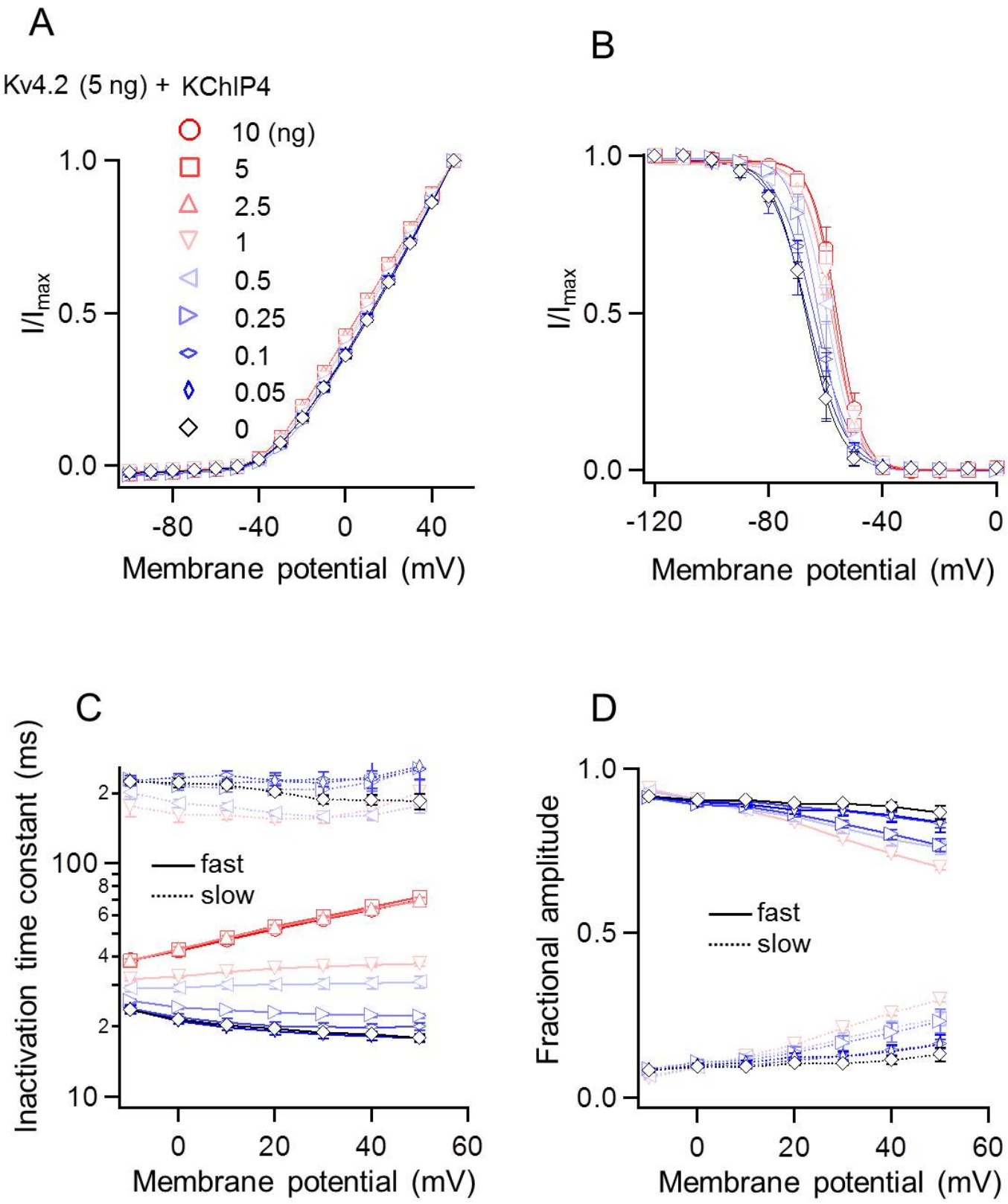
A
Kv4.2 (5 ng) + KChIP4
10 (ng)
5
2.5
1
0.5
0.25
0.1
0.05
0
I/I_max
Membrane potential (mV)
B
I/I_max
Membrane potential (mV)
C
Inactivation time constant (ms)
fast
slow
Membrane potential (mV)
D
Fractional amplitude
fast
slow
Membrane potential (mV)

Figure 5

The recovery from inactivation of Kv4.2 is gradually accelerated with increase in the KChIP4 co-expression.

(A) The representative current traces of Kv4.2 (5 ng) with KChIP4 (0, 0.05, 0.5, 5 ng) are shown. The currents were evoked by a two-pulse protocol shown below. Holding potential was at -80 mV. (B) The kinetics of the recovery from inactivation of Kv4.2 with various expression levels of KChIP4 are shown. The peak current amplitude at second +40 mV stimulation were normalized by the average of the peak current amplitude at +40 mV pre-pulse. The normalized currents at 10, 100, 200, 300, 400, 500, 600, 700, 800 ms of the hyperpolarized duration were shown (n = 3-13). (C) The time constants of the recovery from inactivation of Kv4.2 with various amounts of KChIP4 were plotted. The time constants were obtained from (B) by fitting the curves with a single exponential function. Error bars indicate S.E.

Figure. 5

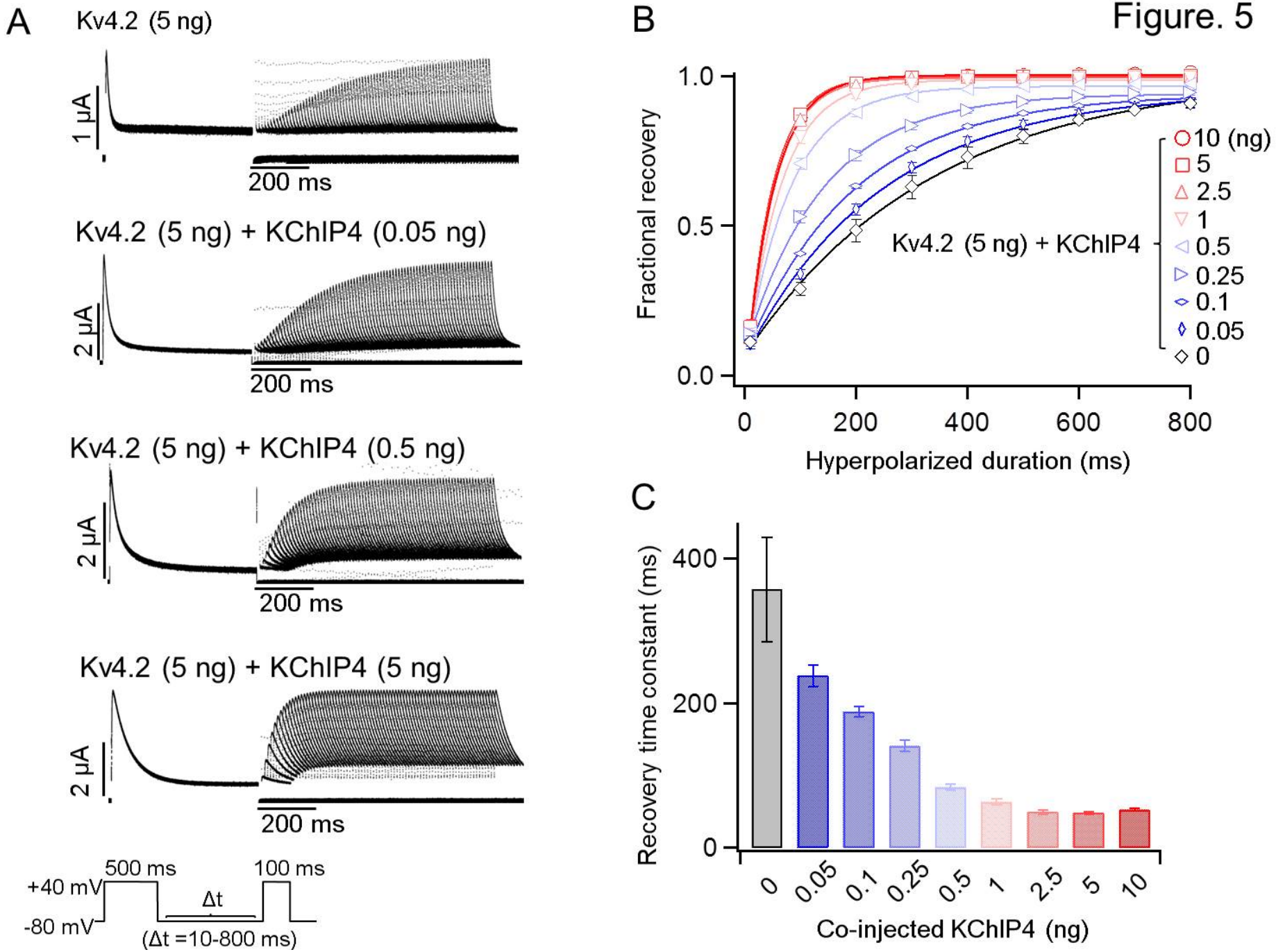
A
Kv4.2 (5 ng)
1 μA
200 ms
Kv4.2 (5 ng) + KChIP4 (0.05 ng)
2 μA
200 ms
Kv4.2 (5 ng) + KChIP4 (0.5 ng)
2 μA
200 ms
Kv4.2 (5 ng) + KChIP4 (5 ng)
2 μA
200 ms
500 ms
100 ms
+40 mV
-80 mV
Δt
(Δt =10-800 ms)
B
Fractional recovery
1.0
0.5
0.0
0
200
400
600
800
Hyperpolarized duration (ms)
Kv4.2 (5 ng) + KChIP4
10 (ng)
5
2.5
1
0.5
0.25
0.1
0.05
0
C
Recovery time constant (ms)
400
200
0
0
0.05
0.1
0.25
0.5
1
2.5
5
10
Co-injected KChIP4 (ng)

Figure 6

The tandem repeat constructs form the 4:2 or the 4:4 (Kv4.2:KChIP4) channel complex.

(A) The schematic illustrations of the tandem repeat constructs. Because Kv4.2 forms a tetramer, KChIP4-Kv4.2-Kv4.2 forms the 4:2 (Kv4.2:KChIP4) channel and KChIP4-Kv4.2 forms the 4:4 channel. (B) The representative current traces of the 4:2 and the 4:4 channel evoked by step pulses from -100 mV to +50 mV in 10 mV increments.

Figure. 6

A

KChIP4-Kv4.2-Kv4.2 (Kv4.2 : KChIP4 = 4 : 2)

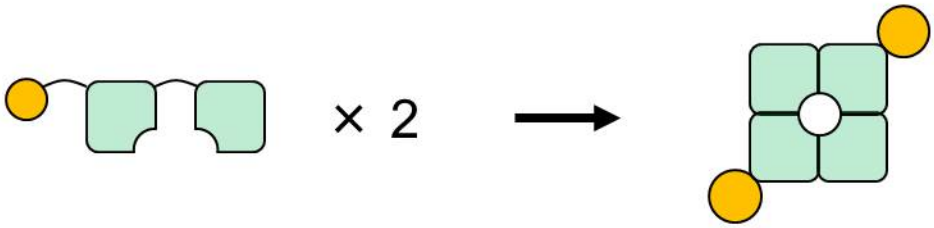

KChIP4-Kv4.2 (Kv4.2 : KChIP4 = 4 : 4)

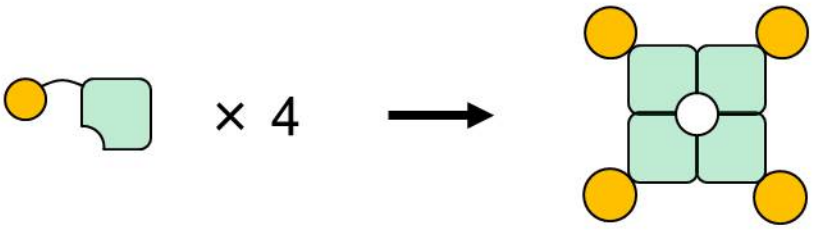

B

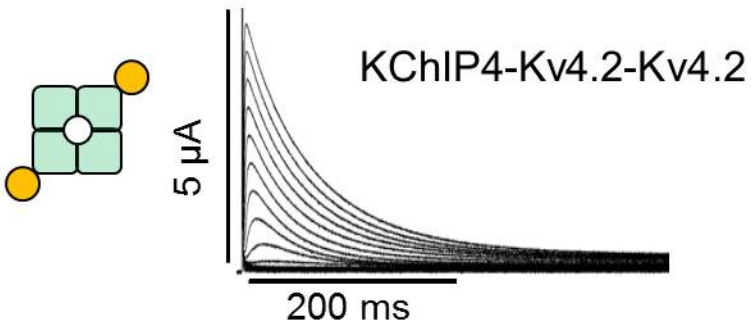

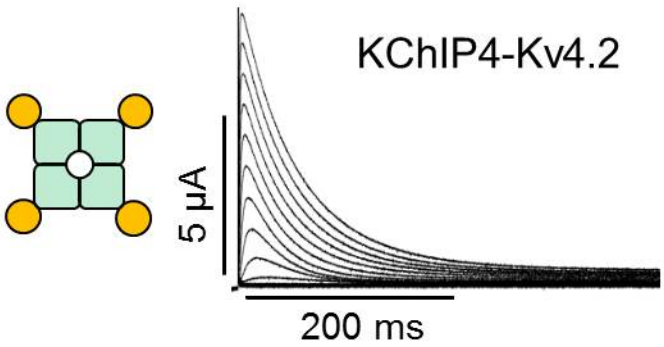

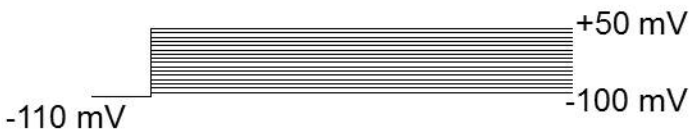

Figure 7

Biophysical properties of the 4:2 and the 4:4 (Kv4.2:KChIP4) channels.

The peak current amplitudes at +40 mV of the 4:2 channel (black bar) and the 4:4 channel (white bar) are plotted (n = 5 for each). (B) I-V relationships for the 4:2 channel (filled triangles) and the 4:4 channel (open circles) are shown. The peak currents at each potential were normalized by the peak current at +50 mV (n = 4 for each). (C) The inactivation time constants of the 4:2 channel (filled triangles, n = 3) and the 4:4 channel (open circles, n = 4) are shown. Time constants were obtained by fitting the inactivating current traces (Fig. 6B) with a single exponential function. (D) The steady-state inactivation curves of the 4:2 channel (filled triangles, n = 3) and the 4:4 channel (open circles, n = 4) are shown.

Figure. 7

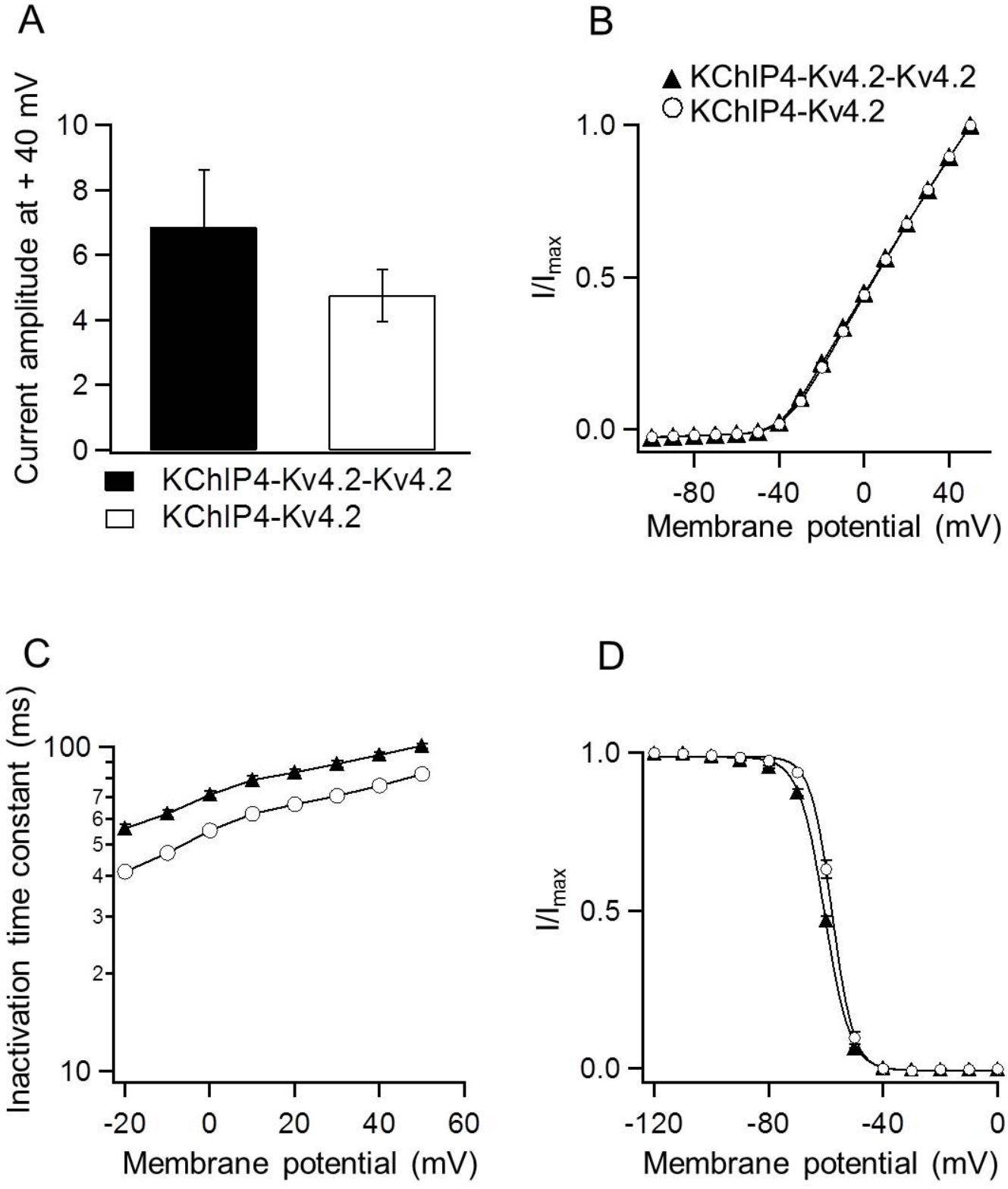
A
Current amplitude at + 40 mV
10
8
6
4
2
0
KChIP4-Kv4.2-Kv4.2
KChIP4-Kv4.2
B
KChIP4-Kv4.2-Kv4.2
KChIP4-Kv4.2
1.0
0.5
0.0
I/I_max
-80
-40
0
40
Membrane potential (mV)
C
Inactivation time constant (ms)
100
7
6
5
4
3
2
10
-20
0
20
40
60
Membrane potential (mV)
D
1.0
0.5
0.0
I/I_max
-120
-80
-40
0
Membrane potential (mV)

Figure 8

The 4:4 (Kv4.2:KChIP4) channel shows faster recovery from inactivation than the 4:2 channel.

(A) The representative current traces of the 4:2 (top) and the 4:4 channel (botttom) are shown. The currents were evoked by a two-pulse protocol as shown below. (B) The kinetics of the recovery from inactivation of the 4:4 channel (n = 4), the 4:2 channel (n = 4), the 4:2 channel with additional KChIP4 (n = 4), Kv4.2 (5 ng) with KChIP4 (5 or 0.5 ng) (n = 4 for each) and Kv4.2 alone (5 ng) (n = 6) are plotted. The peak current amplitudes at +40 mV test pulse after hyperpolarization were normalized by the average of the pre-pulse current amplitude at +40 mV. (C) Time constants of the recovery from inactivation from (B) were plotted. *** shows the statistically significant difference $P < 0.001$. Error bars show S.E.

Figure. 8

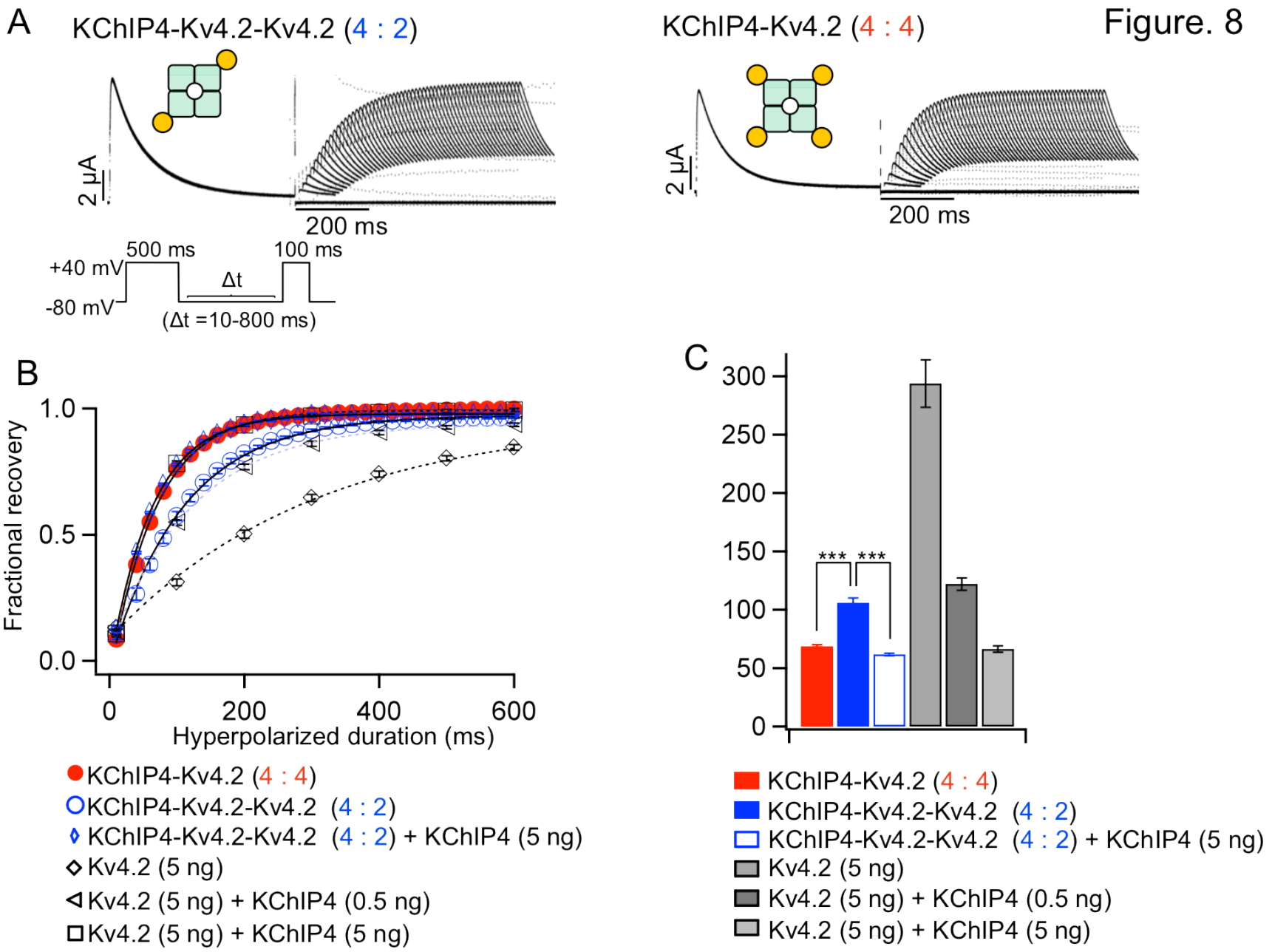
A
KChIP4-Kv4.2-Kv4.2 (4 : 2)
KChIP4-Kv4.2 (4 : 4)
2 μA
200 ms
500 ms
100 ms
+40 mV
Δt
-80 mV
(Δt =10-800 ms)
B
Fractional recovery
1.0
0.5
0.0
0
200
400
600
Hyperpolarized duration (ms)
KChIP4-Kv4.2 (4 : 4)
KChIP4-Kv4.2-Kv4.2 (4 : 2)
KChIP4-Kv4.2-Kv4.2 (4 : 2) + KChIP4 (5 ng)
Kv4.2 (5 ng)
Kv4.2 (5 ng) + KChIP4 (0.5 ng)
Kv4.2 (5 ng) + KChIP4 (5 ng)
C
300
250
200
150
100
50
0
***
***
KChIP4-Kv4.2 (4 : 4)
KChIP4-Kv4.2-Kv4.2 (4 : 2)
KChIP4-Kv4.2-Kv4.2 (4 : 2) + KChIP4 (5 ng)
Kv4.2 (5 ng)
Kv4.2 (5 ng) + KChIP4 (0.5 ng)
Kv4.2 (5 ng) + KChIP4 (5 ng)

Figure 9

Kv4.2 forms a tetramer.

(A) The schematic illustration of Kv4.2-mEGFP. mEGFP was tagged to the C-terminus of Kv4.2. The representative current traces of Kv4.2 and Kv4.2-mEGFP evoked by the step pulse protocol as used in Figure 1A, 2A and 6B are shown. (B) A single frame from a movie of Kv4.2-mEGFP expressed in *Xenopus* oocyte under TIRF microscope. Green circles show the countable spots for analysis. White bar indicates 2 μm. (C) The representative fluorescent traces showing four, three, two and one bleaching steps are shown. The green bars indicate the continuous excitation by a 488-nm laser. The green arrows indicate the bleaching events. (D) The distribution of the number of bleaching steps from each spot is plotted. The green bar shows the observed distribution and white bar shows the fitting with a binomial distribution with p = 76%. p is the fluorescent probability of mEGFP attached to Kv4.2.

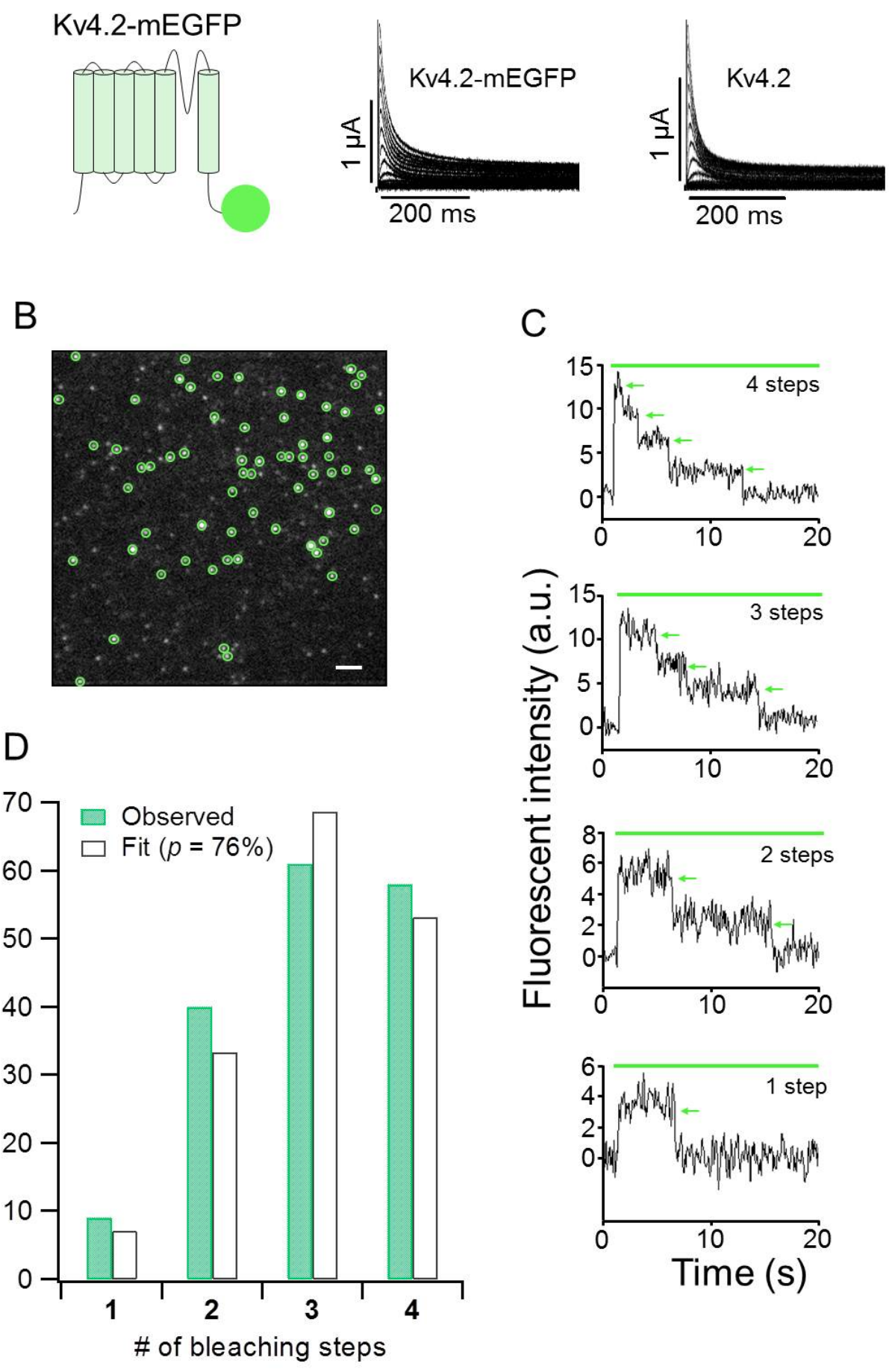
A
Kv4.2-mEGFP
Kv4.2-mEGFP
1 μA
200 ms
Kv4.2
1 μA
200 ms
B
C
4 steps
3 steps
2 steps
1 step
Fluorescent intensity (a.u.)
Time (s)
D
Observed
Fit (p = 76%)
# of spots
# of bleaching steps

Figure 10

The stoichiometry of Kv4.2/KChIP4 complex changes with the co-expression level of KChIP4.

(A) The schemes of Kv4.2 and KChIP4-mEGFP are shown. mEGFP was fused to the C-terminus of KChIP4. (B) The representative current traces of Kv4.2 (5 ng) with KChIP4-mEGFP (5 ng) (top) and Kv4.2 (5 ng) with wild-type KChIP4 (5 ng) (bottom) are shown. The currents were elicited by step pulses between -100 mV and +50 mV in 10 ms increments. (C) A single image from the movie of the oocyte expressing Kv4.2 and KChIP4-mEGFP taken under TIRF microscope. The green circles indicate countable fluorescent spots of KChIP4-mEGFP. Scale bar indicates 2 μm. (D) The representative bleaching traces of KChIP4-mEGFP with four, three, two and one bleaching steps. The green bar indicates the illumination with a 488-nm laser and the green arrows indicate the bleaching steps. (E) The distributions of the number of the bleaching steps with different ratios of Kv4.2 and KChIP4-mEGFP cRNA (100 : 1, 10 : 1, 1 : 1) are plotted (red bars). The distributions are fitted with a binomial distribution with an apparent fluorescent probability (p'), which is the product of (fluorescent probability of mEGFP)×(association probability of KChIP4-mEGFP with Kv4.2) (blue bars). The experiment was repeated twice in the same conditions

Figure. 10

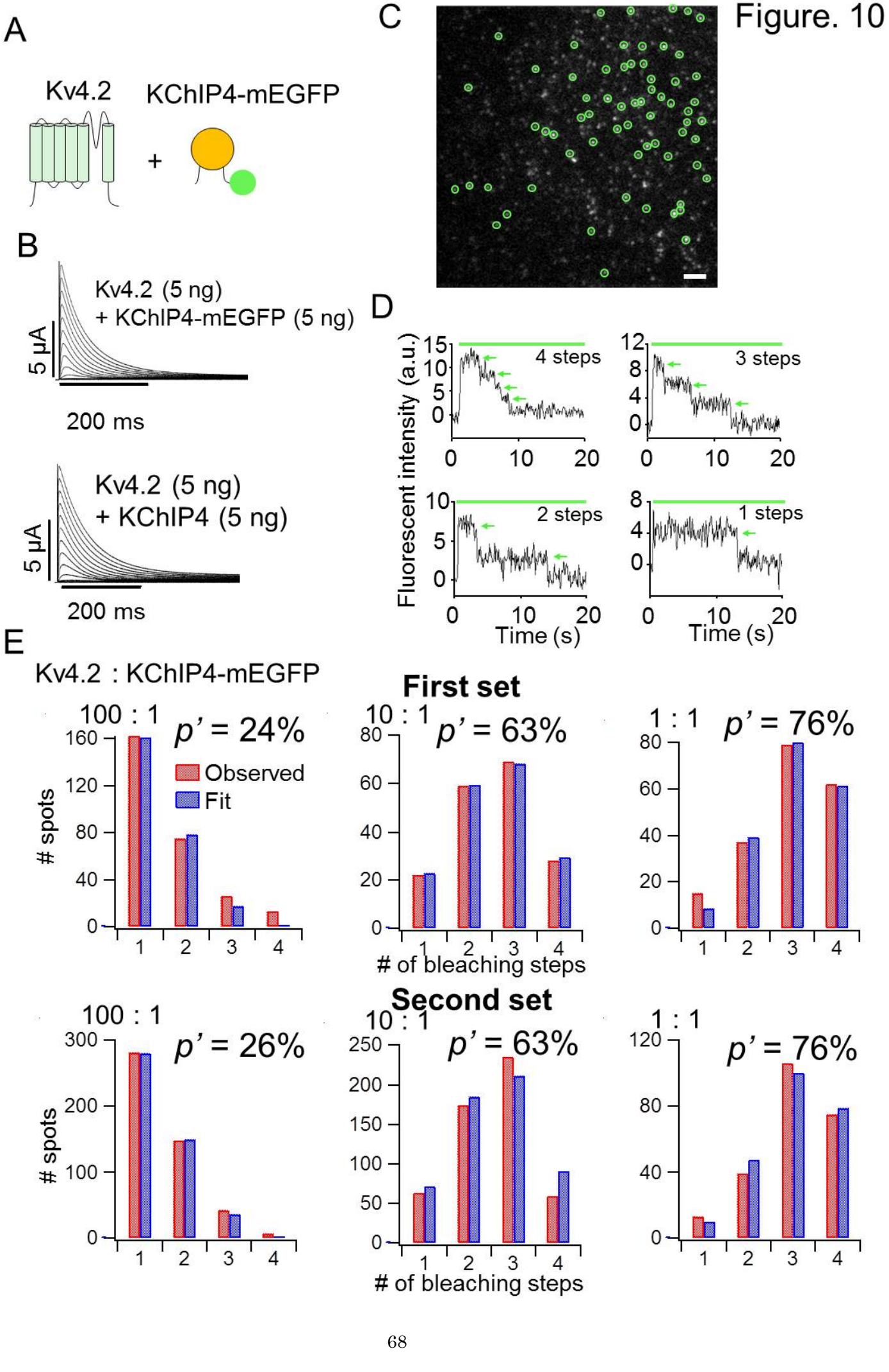
A
Kv4.2
KChIP4-mEGFP
+
B
Kv4.2 (5 ng)
+ KChIP4-mEGFP (5 ng)
5 μA
200 ms
Kv4.2 (5 ng)
+ KChIP4 (5 ng)
5 μA
200 ms
C
D
Fluorescent intensity (a.u.)
4 steps
3 steps
2 steps
1 steps
Time (s)
Time (s)
E
Kv4.2 : KChIP4-mEGFP
First set
100 : 1
p' = 24%
Observed
Fit
spots
10 : 1
p' = 63%
1 : 1
p' = 76%
# of bleaching steps
Second set
100 : 1
p' = 26%
spots
10 : 1
p' = 63%
1 : 1
p' = 76%
# of bleaching steps

Figure 11

Fluorescent probability of mEGFP attached to KChIP4 is 77%.

(A) The scheme of Kv4.2-KChIP4-mEGFP tandem repeat construct. Kv4.2, KChIP4 and mEGFP are linked with flexible GGS linkers. (B) A single frame of the fluorescent movie from the *Xenopus* oocyte expressing Kv4.2-KChIP4-mEGFP is shown. The green circles indicate the spots used for counting the bleaching steps. (C) The distribution of each bleaching step was fitted with a binomial distribution with p (77%) of the fluorescent probability of mEGFP attached to KChIP4. (D) The association probabilities of KChIP4 with Kv4.2 for each cRNA ratios are calculated by dividing p' taken from Fig. 10E by fluorescent probability of mEGFP attached to KChIP4 (77%).

Figure. 11

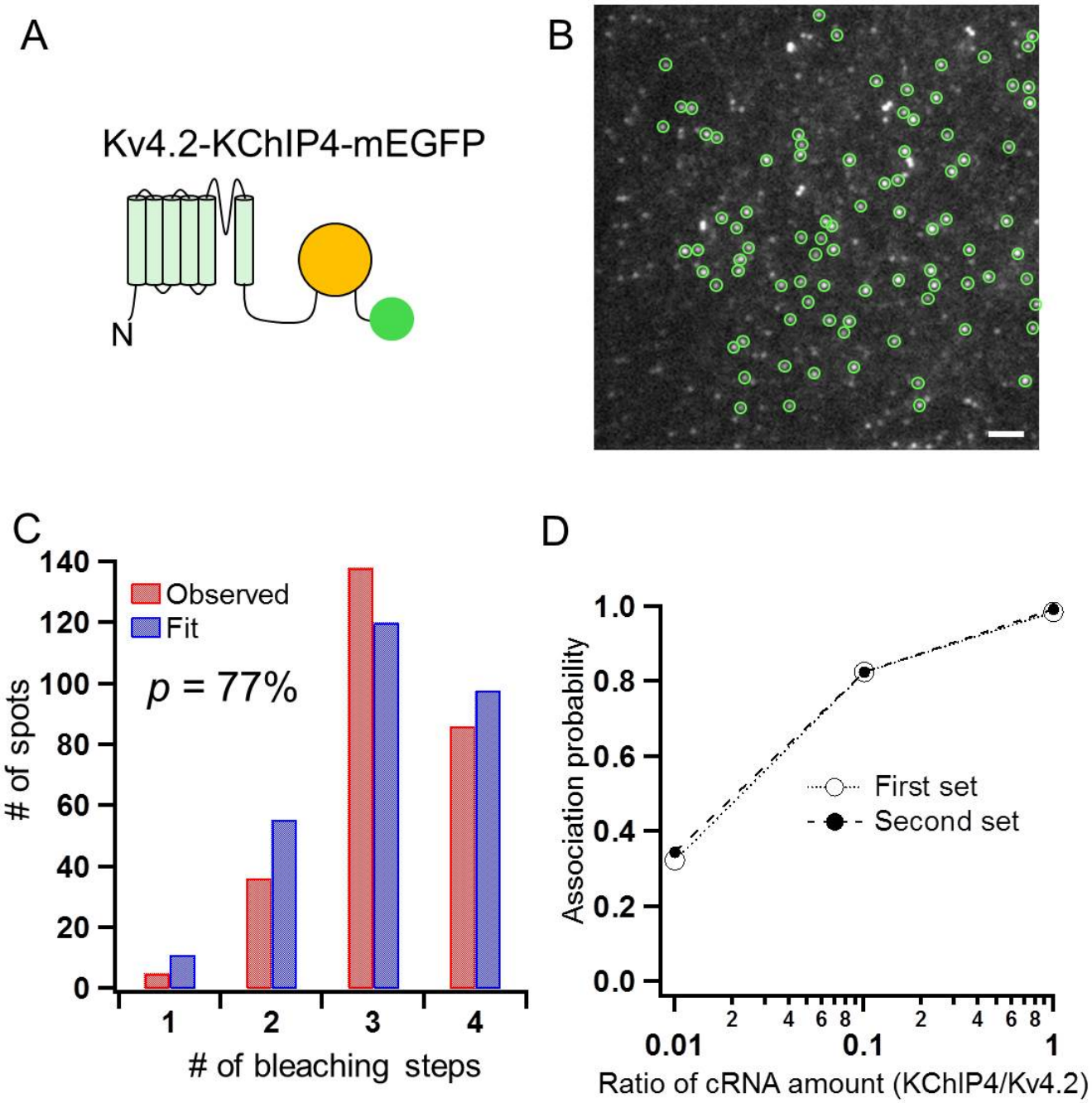
A
Kv4.2-KChIP4-mEGFP
N
B
C
Observed
Fit
p = 77%
# of spots
140
120
100
80
60
40
20
0
1
2
3
4
# of bleaching steps
D
Association probability
1.0
0.8
0.6
0.4
0.2
0.0
First set
Second set
0.01
0.1
1
Ratio of cRNA amount (KChIP4/Kv4.2)

Figure 12

Expression of DPP10 does not affect the stoichiometry of Kv4.2/KChIP4 complex.

(A) Kv4.2, KChIP4-mEGFP and DPP10 all were expressed together in *Xenopus* oocyte. (B) The representative current traces of Kv4.2 and KChIP4 in the absence (left) and the presence (right) of DPP10. (C) The distributions of the bleaching steps with each cRNA ratios are represented and fitted with a binomial distribution with *p'* (27% for Kv4.2 : KChIP4 : DPP10 = 100 : 1 : 100, 69% for 10 : 1 : 10). (D) Association probabilities of the KChIP4 with Kv4.2 in the presence of DPP10 are calculated. The association probabilities were 36% (Kv4.2 : KChIP4-mEGFP : DPP10 = 100 : 1 : 100,) and 90% (10 : 1 : 10).

Figure. 12

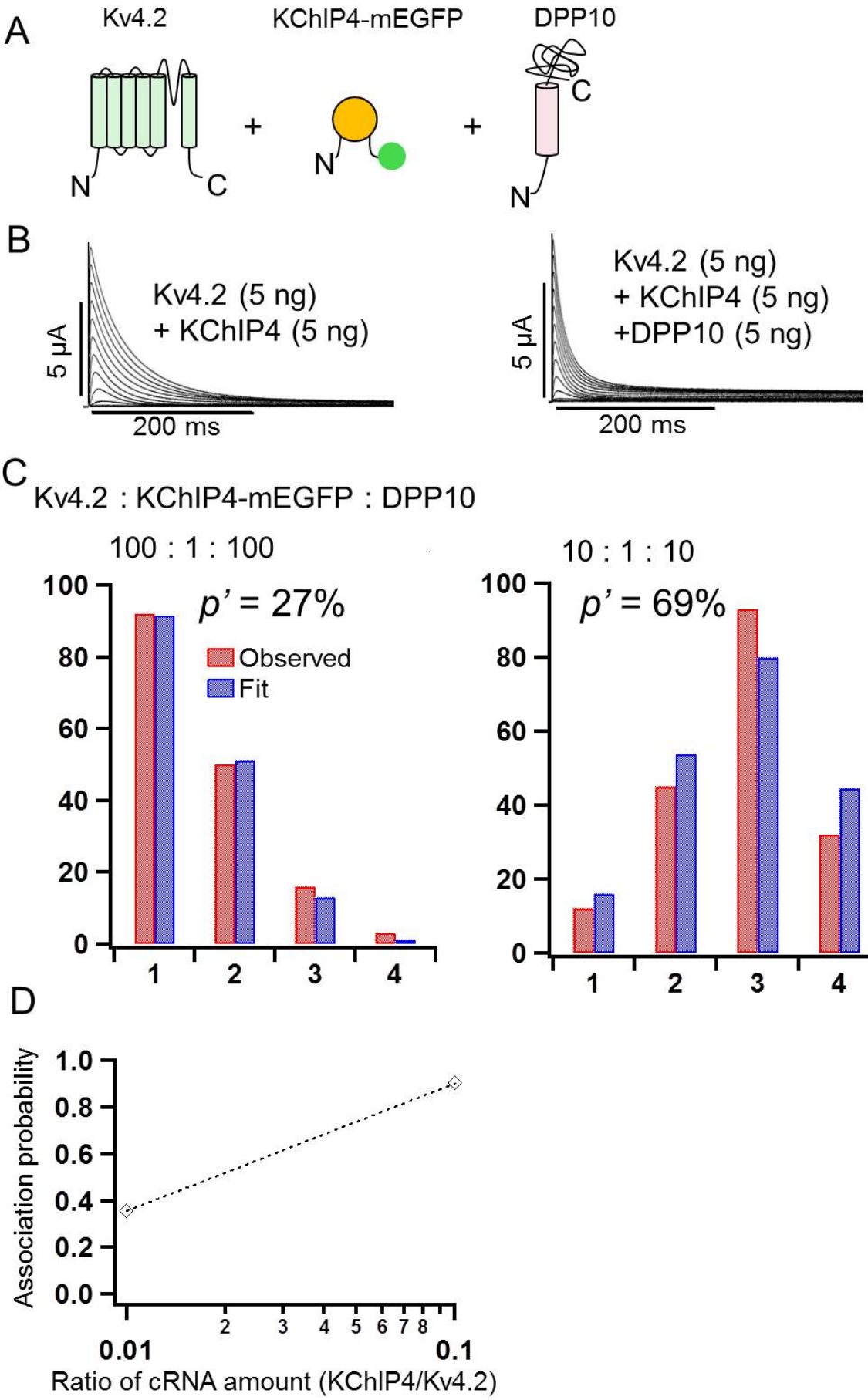
A
Kv4.2
KChIP4-mEGFP
DPP10
N
C
+
+
B
Kv4.2 (5 ng)
+ KChIP4 (5 ng)
5 μA
200 ms
Kv4.2 (5 ng)
+ KChIP4 (5 ng)
+DPP10 (5 ng)
C
Kv4.2 : KChIP4-mEGFP : DPP10
100 : 1 : 100
p' = 27%
Observed
Fit
10 : 1 : 10
p' = 69%
D
Association probability
Ratio of cRNA amount (KChIP4/Kv4.2)

Figure 13

The expression level of DPP10 affects the current amplitude of Kv4.2.

(A) The representative current traces of Kv4.2 (2.5 ng) with DPP10 (0, 0.025, 0.25 and 2.5 ng) are shown. The currents were elicited by step pluses as shown in the inset. (B) The current amplitudes of Kv4.2 with various expression levels of DPP10 are compared (n = 10-19). (C) I-V relationships of Kv4.2 with various amounts of DPP10 cRNA are shown. The peak current amplitudes at each potential taken from (A) are normalized by the peak current amplitude at +50 mV (n = 10-19).

Figure. 13

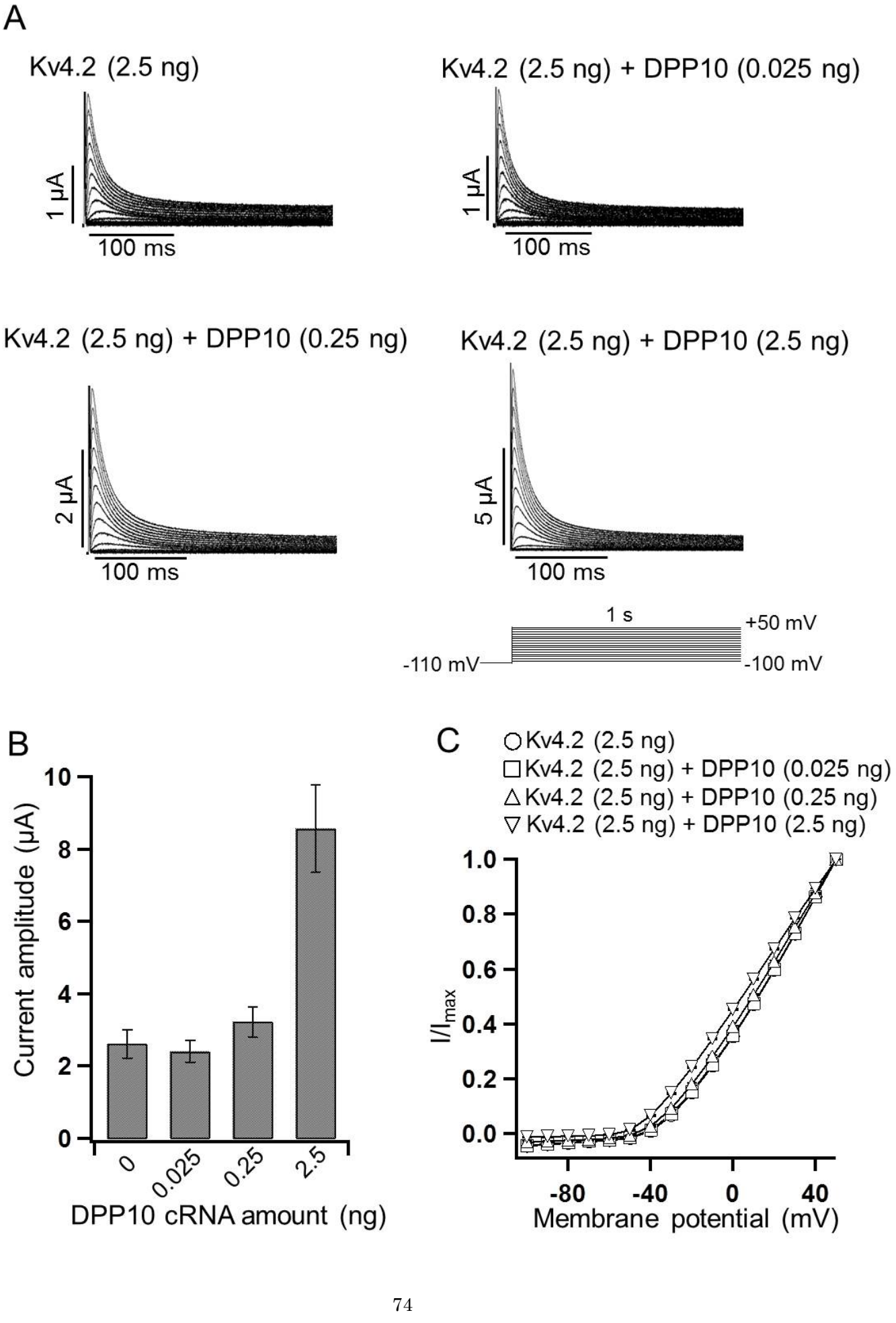
A
Kv4.2 (2.5 ng)
1 μA
100 ms
Kv4.2 (2.5 ng) + DPP10 (0.025 ng)
1 μA
100 ms
Kv4.2 (2.5 ng) + DPP10 (0.25 ng)
2 μA
100 ms
Kv4.2 (2.5 ng) + DPP10 (2.5 ng)
5 μA
100 ms
1 s
+50 mV
-110 mV
-100 mV
B
Current amplitude (μA)
10
8
6
4
2
0
0
0.025
0.25
2.5
DPP10 cRNA amount (ng)
C
Kv4.2 (2.5 ng)
Kv4.2 (2.5 ng) + DPP10 (0.025 ng)
Kv4.2 (2.5 ng) + DPP10 (0.25 ng)
Kv4.2 (2.5 ng) + DPP10 (2.5 ng)
I/I_max
1.0
0.8
0.6
0.4
0.2
0.0
-80
-40
0
40
Membrane potential (mV)

Figure 14

The biophysical properties of Kv4.2 are affected by the co-expressed amount of DPP10.

(A) The inactivation time constants of Kv4.2 without DPP10 (open circles) and with DPP10 (0.025 ng, open squares), (0.25 ng, open triangles) and (2.5 ng, open inverted triangles) are compared (n = 5-10). The inactivation kinetics is fitted with a double exponential function and both of the fast and slow time constants are plotted. (B) Fractional contribution of the fast and slow inactivation time constants. (C) The steady state inactivation curves of Kv4.2 with different expression ratios of Kv4.2 and DPP10 are shown (n = 6-9). (D) Times for reaching peak current (time to peak) upon initiation of test pulse are plotted for each cRNA ratios.

Figure. 14

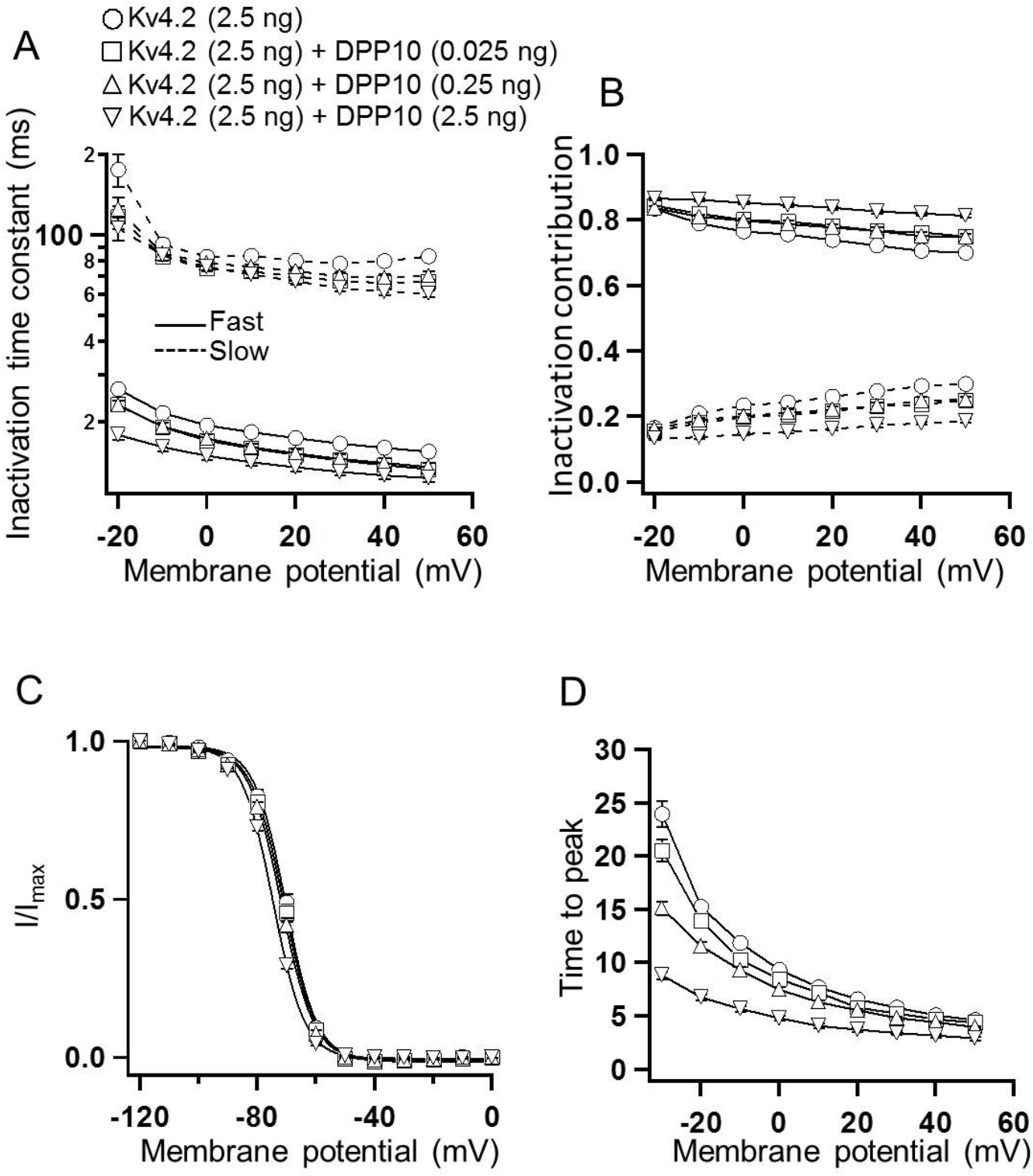
A
Kv4.2 (2.5 ng)
Kv4.2 (2.5 ng) + DPP10 (0.025 ng)
Kv4.2 (2.5 ng) + DPP10 (0.25 ng)
Kv4.2 (2.5 ng) + DPP10 (2.5 ng)
Inactivation time constant (ms)
Fast
Slow
Membrane potential (mV)
B
Inactivation contribution
Membrane potential (mV)
C
I/I_max
Membrane potential (mV)
D
Time to peak
Membrane potential (mV)

Figure 15

The recovery from inactivation of Kv4.2 is gradually accelerated along with increase in the expression level of DPP10.

(A) The representative current traces of the recovery from inactivation are shown. Various amounts of DPP10 cRNA (0, 0.025, 0.25 and 2.5 ng) were co-injected with 2.5 ng of Kv4.2 cRNA. The currents were elicited by a two-pulse protocol. Holding potential was -100 mV. (B) The kinetics of the recovery from inactivation of Kv4.2 with various expression levels of DPP10 are shown (n = 7-9). The peak current amplitude at second +40 mV stimulation was normalized by the average of the peak current amplitude at +40 mV pre-pulse. (C) Time constants of the recovery from inactivation of Kv4.2 with the different DPP10 expression amount are compared. The time constants are obtained by fitting the curves taken from (B) with a single exponential. Error bars are S.E.

Figure. 15

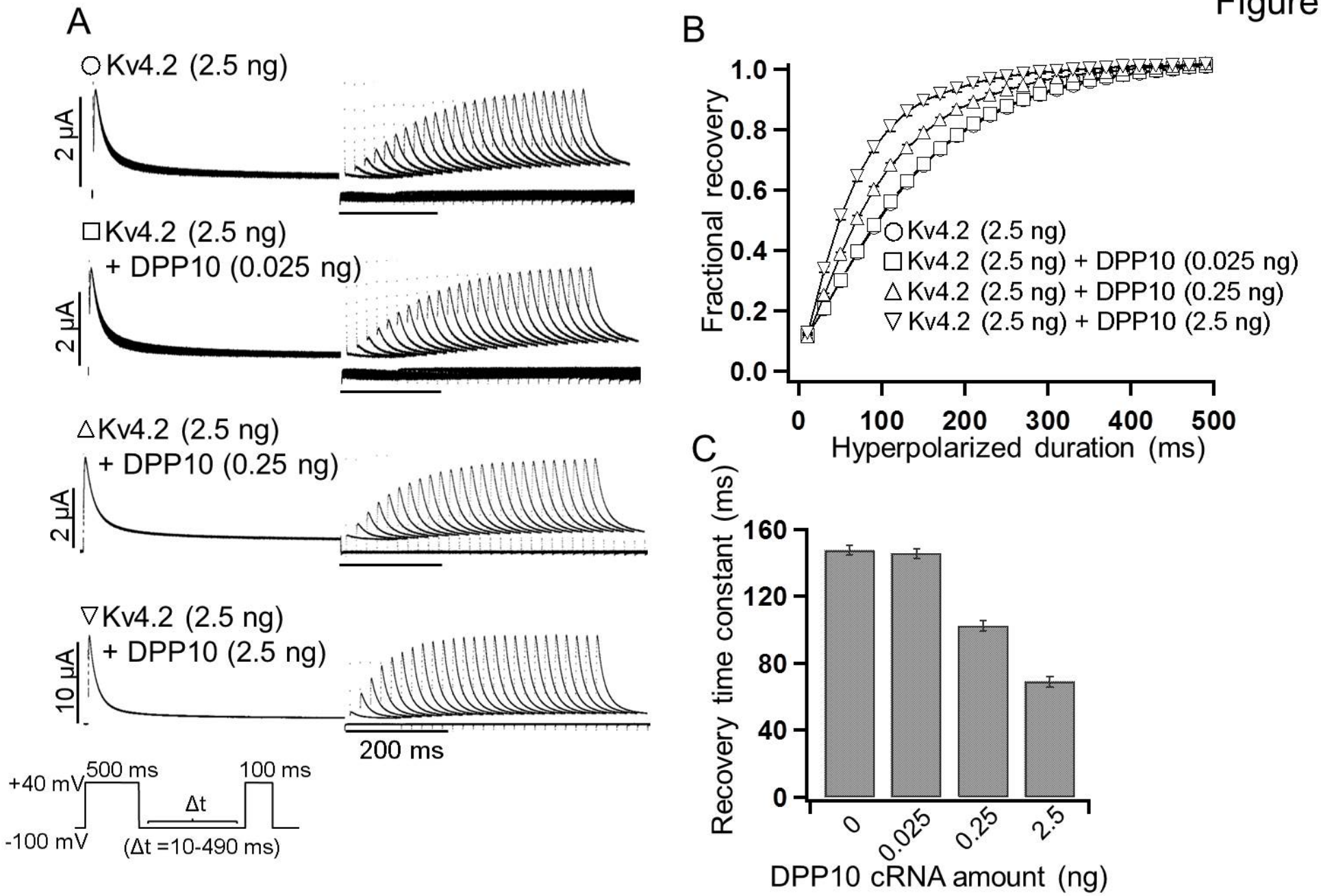
A
Kv4.2 (2.5 ng)
2 μA
Kv4.2 (2.5 ng)
+ DPP10 (0.025 ng)
2 μA
Kv4.2 (2.5 ng)
+ DPP10 (0.25 ng)
2 μA
Kv4.2 (2.5 ng)
+ DPP10 (2.5 ng)
10 μA
200 ms
+40 mV
500 ms
100 ms
Δt
-100 mV
(Δt =10-490 ms)
B
Fractional recovery
1.0
0.8
0.6
0.4
0.2
0.0
0
100
200
300
400
500
Hyperpolarized duration (ms)
Kv4.2 (2.5 ng)
Kv4.2 (2.5 ng) + DPP10 (0.025 ng)
Kv4.2 (2.5 ng) + DPP10 (0.25 ng)
Kv4.2 (2.5 ng) + DPP10 (2.5 ng)
C
Recovery time constant (ms)
160
120
80
40
0
0
0.025
0.25
2.5
DPP10 cRNA amount (ng)

Figure 16

Approximately 70% of DPP10 complex exist as dimers.

(A) The schematic illustration of DPP10-mEGFP is shown. mEGFP was fused to the N terminus of DPP10, which is an intracellular side. (B) A single frame of the TIRF movie from the *Xenopus* oocyte expressing DPP10-mEGFP is shown. The green circles indicate the fluorescent spots of DPP10-mEGFP. Scale bar is 2 μm. (C) The representative fluorescent traces taken from the fluorescent spots in (B) are shown. The green bar shows the time of illumination with a 488-nm laser. The green arrows indicate the bleaching steps. (D) The observed distribution of the number of bleaching steps is plotted as histogram. (E) The proportions of dimer and monomer DPP10 based on the distribution in (D). The value of fluorescent probability of mEGFP (p) was changed between 0.63 and 1. (F) The schematic illustrations of dimer DPP10 and monomer DPP10. If p is assumed to be between 70%-80%, approximately 70% of DPP exist as a dimer and 30% of DPP exist as a monomer.

Figure. 16

A

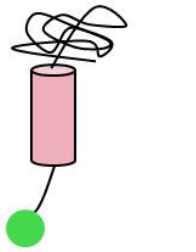

B

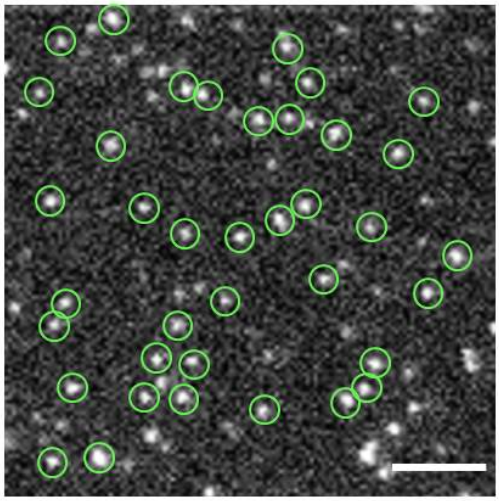

C

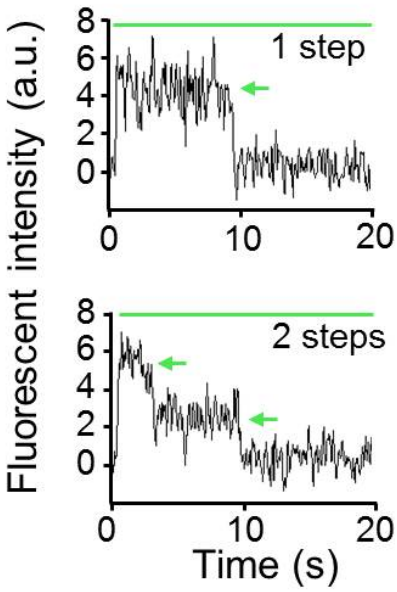

D

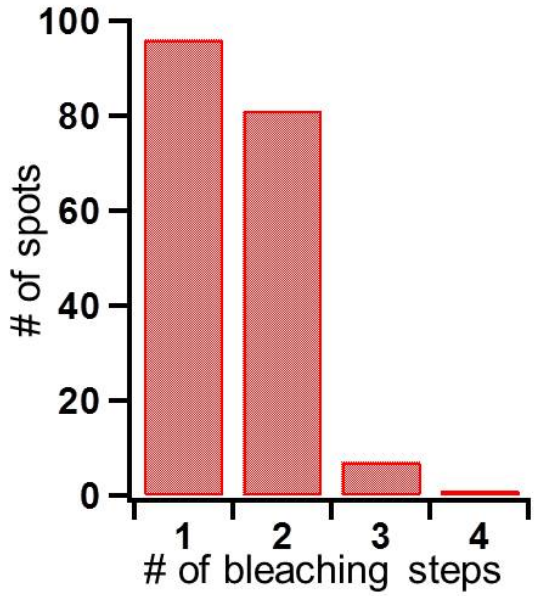

E

p	Dimer	Monomer
1	0.46	0.54
0.9	0.54	0.46
0.8	0.65	0.35
0.7	0.81	0.19
0.63	0.99	0.01

(fluorescent probability of mEGFP = *p*)

F

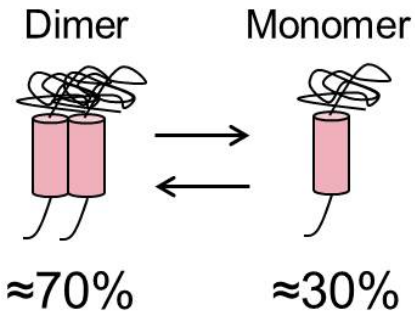

Figure 17

Confirmation of co-localization of Kv4.2 and DPP10.

(A) The schematic illustrations of Kv4.2-mCherry and DPP10-mEGFP. mCherry is fused to the C-terminus of Kv4.2 and mEGFP is fused to the N-terminus of DPP10. (B) The representative current traces of Kv4.2 (2.5 ng) with DPP10 (2.5 ng) (top) and Kv4.2-mCherry (2.5 ng) with DPP10-mEGFP (2.5 ng) (bottom) are shown. (C) Image of fluorescent spots of Kv4.2-mCherry is shown. (D) Image of fluorescent spots of DPP10-mEGFP is shown. (E) The images from (C) and (D) are overlaid. The white arrowheads (yellow spots) indicate the co-localization of Kv4.2-mCherry and DPP10-mEGFP. Scale bars are 2 μm.

Figure. 17

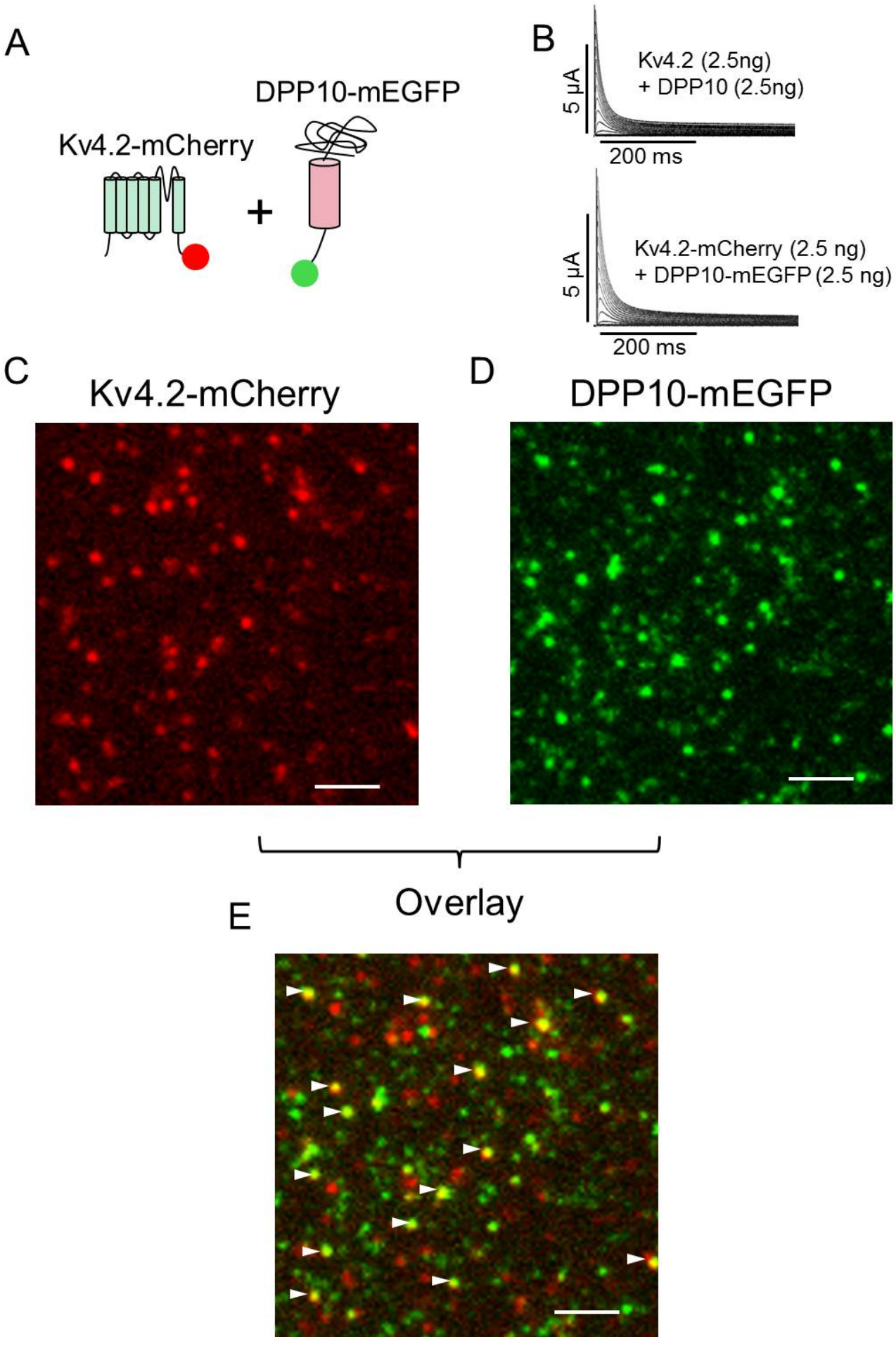
A
DPP10-mEGFP
Kv4.2-mCherry
+
B
5 μA
Kv4.2 (2.5ng)
+ DPP10 (2.5ng)
200 ms
5 μA
Kv4.2-mCherry (2.5 ng)
+ DPP10-mEGFP (2.5 ng)
200 ms
C
Kv4.2-mCherry
D
DPP10-mEGFP
Overlay
E

Figure 18

The stoichiometry of Kv4.2/DPP10 complex has a preference to 4:2.

(A) The representative fluorescent traces of one, two, three and four bleaching steps are shown. The red bars indicate the illumination with a 588-nm laser and the green bars indicate the illumination with a 488-nm laser. The green arrows show the bleaching steps. (B) The distributions of the number of each bleaching steps are plotted as histograms. Kv4.2-mCherry and DPP10-mEGFP are expressed with different ratios (100 : 1, 10 : 1 and 1 : 1).

Figure. 18

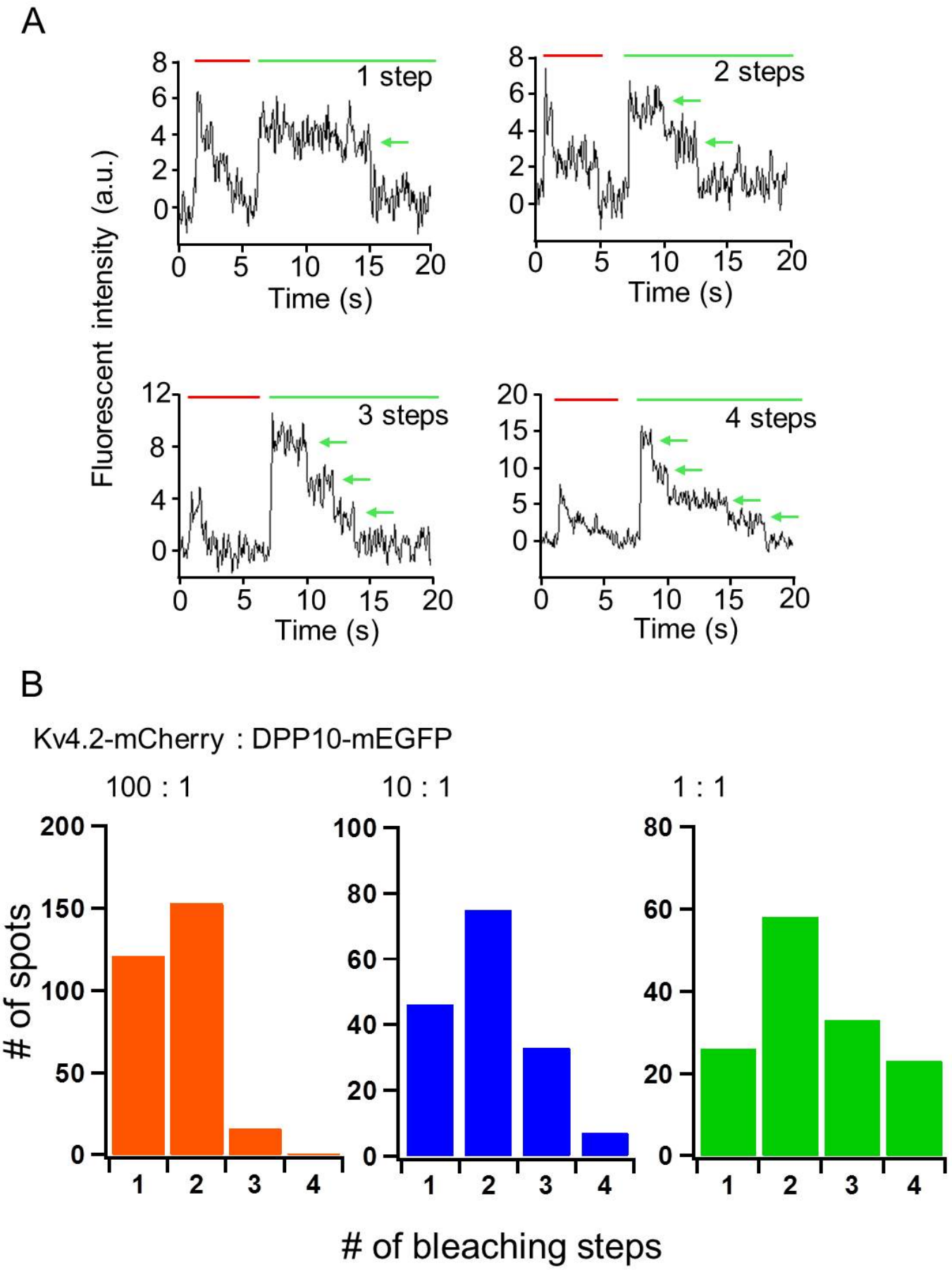
A
Fluorescent intensity (a.u.)
1 step
2 steps
3 steps
4 steps
Time (s)
B
Kv4.2-mCherry : DPP10-mEGFP
100 : 1
10 : 1
1 : 1
# of spots
# of bleaching steps

Figure 19

The co-expression of KChIP4 does not affect the stoichiometry of Kv4.2/DPP10 complex.

(A) The schematic illustrations of Kv4.2-mCherry, KChIP4 and DPP10-mEGFP are shown. (B) Kv4.2-mCherry, KChIP4 and DPP10-mEGFP were expressed in *Xenopus* oocyte with different ratios as shown. Distributions of the bleaching steps from the spots of DPP10-mEGFP are plotted as histograms.

Figure. 19

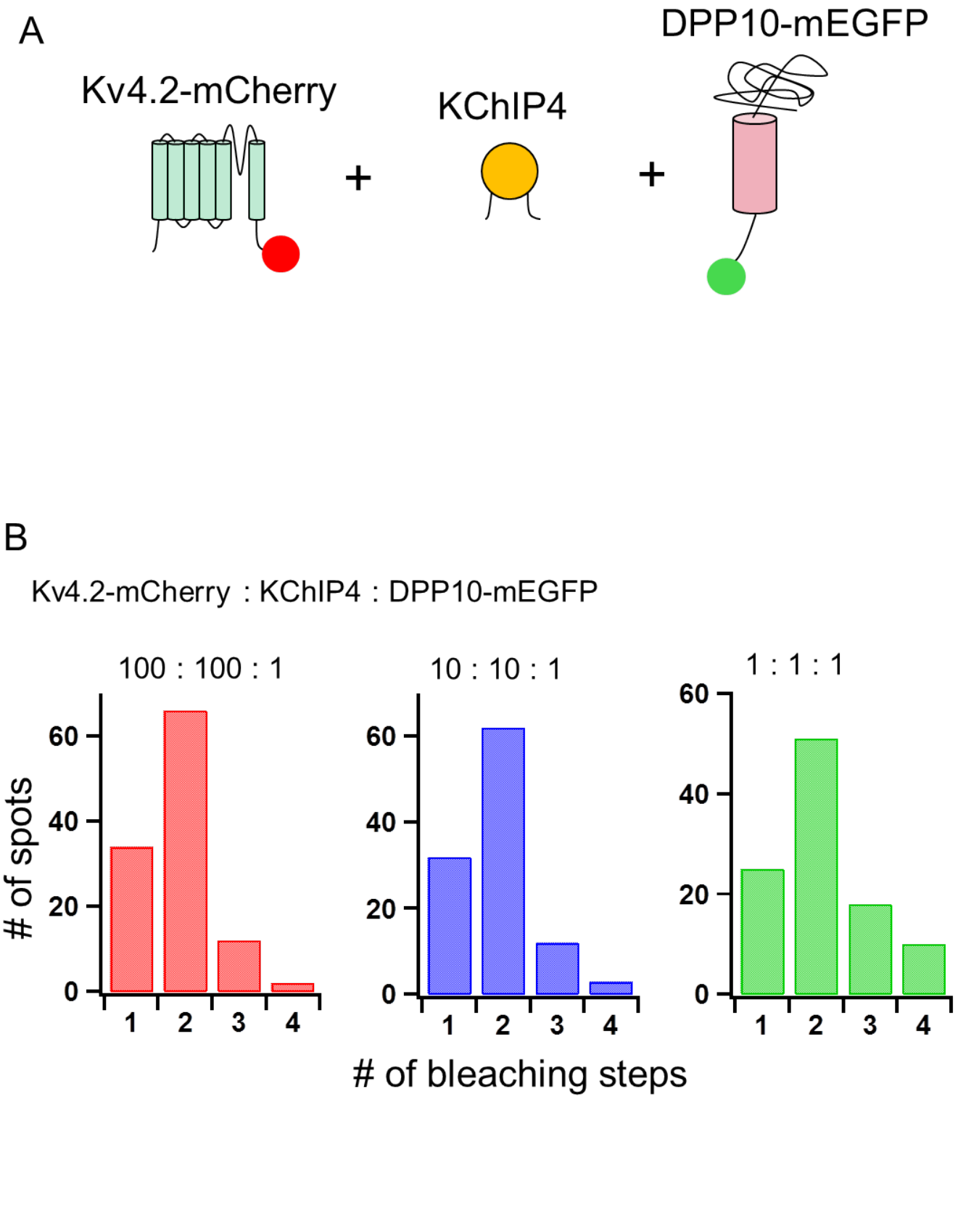
A
Kv4.2-mCherry
KChIP4
DPP10-mEGFP
+
+
B
Kv4.2-mCherry : KChIP4 : DPP10-mEGFP
100 : 100 : 1
10 : 10 : 1
1 : 1 : 1
# of spots
0
20
40
60
1
2
3
4
# of bleaching steps

Figure 20

The schematic illustration of the stoichiometry change in Kv4.2/KChIP4 and Kv4.2/DPP10 complex.

(A) The stoichiometry of Kv4.2/KChIP4 complex changes depending on the relative expression level of Kv4.2 and KChIP4 subunits. KChIP4 can bind to Kv4.2 with no clear preference. (B) Although the stoichiometry of Kv4.2/DPP10 complex changes depending on the relative expression level of Kv4.2 and DPP10 subunits, the stoichiometry of Kv4.2/DPP10 complex shows a clear preference to 4:2.

Figure. 20

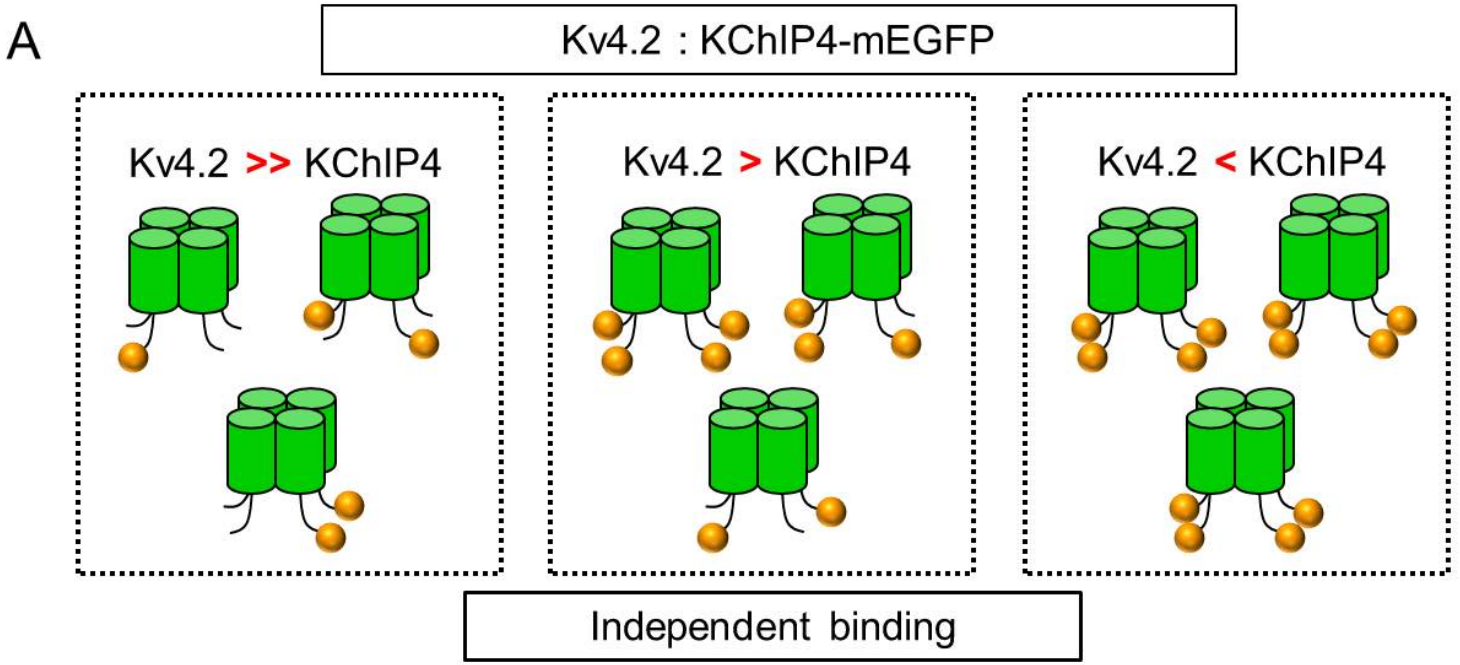
A
Kv4.2 : KChIP4-mEGFP
Kv4.2 >> KChIP4
Kv4.2 > KChIP4
Kv4.2 < KChIP4
Independent binding

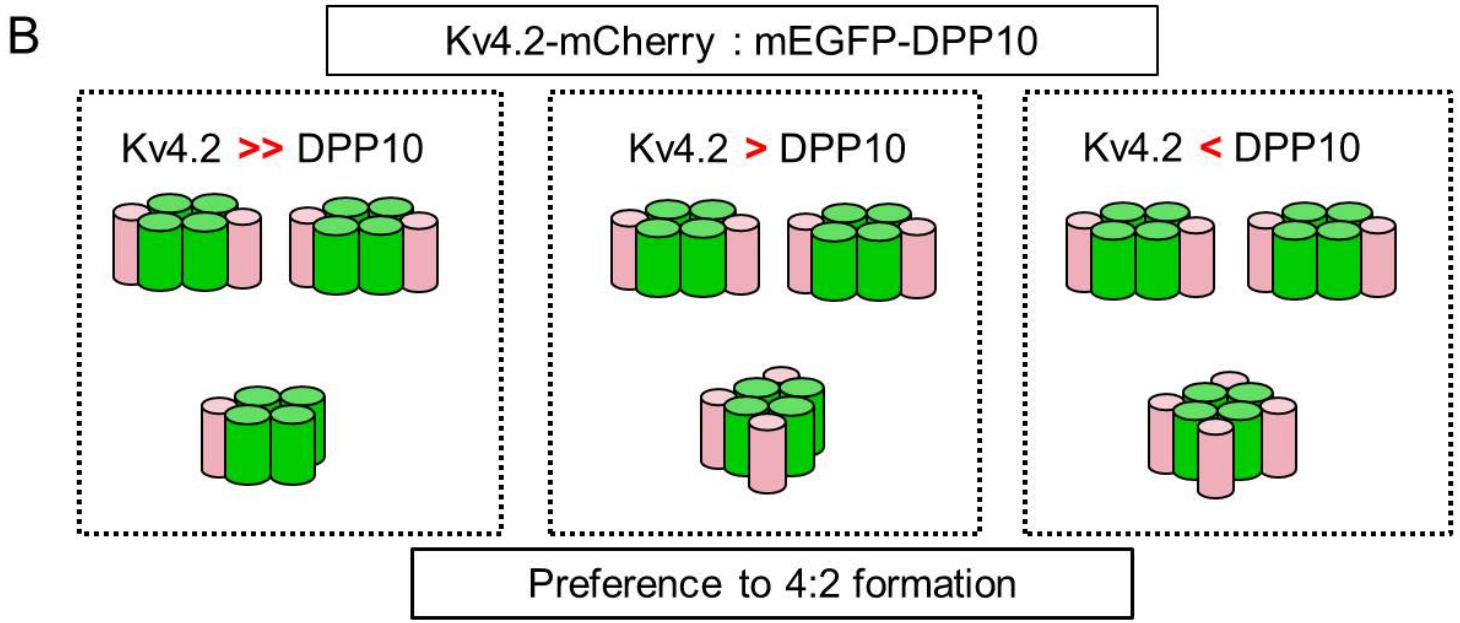
B
Kv4.2-mCherry : mEGFP-DPP10
Kv4.2 >> DPP10
Kv4.2 > DPP10
Kv4.2 < DPP10
Preference to 4:2 formation

Figure 21

The schematic illustrations of Kv4.2/DPP10 complex formed by DPP10 dimer or DPP10 monomer.

DPP10 exists as mixture of dimers and monomers on the plasma membrane. If a dimer binds to Kv4.2, eight DPP10 subunits can bind to a single Kv4.2 channel, but that is not the case according to my subunit counting experiment (left). If a monomer binds to Kv4.2, up to four DPP10 subunits can bind (right). Large extracellular domain may prevent the third and fourth DPP10 from binding to Kv4.2 channel. This may be why the 4:2 stoichiometry is preferred in Kv4/DPP complex.

Figure. 21

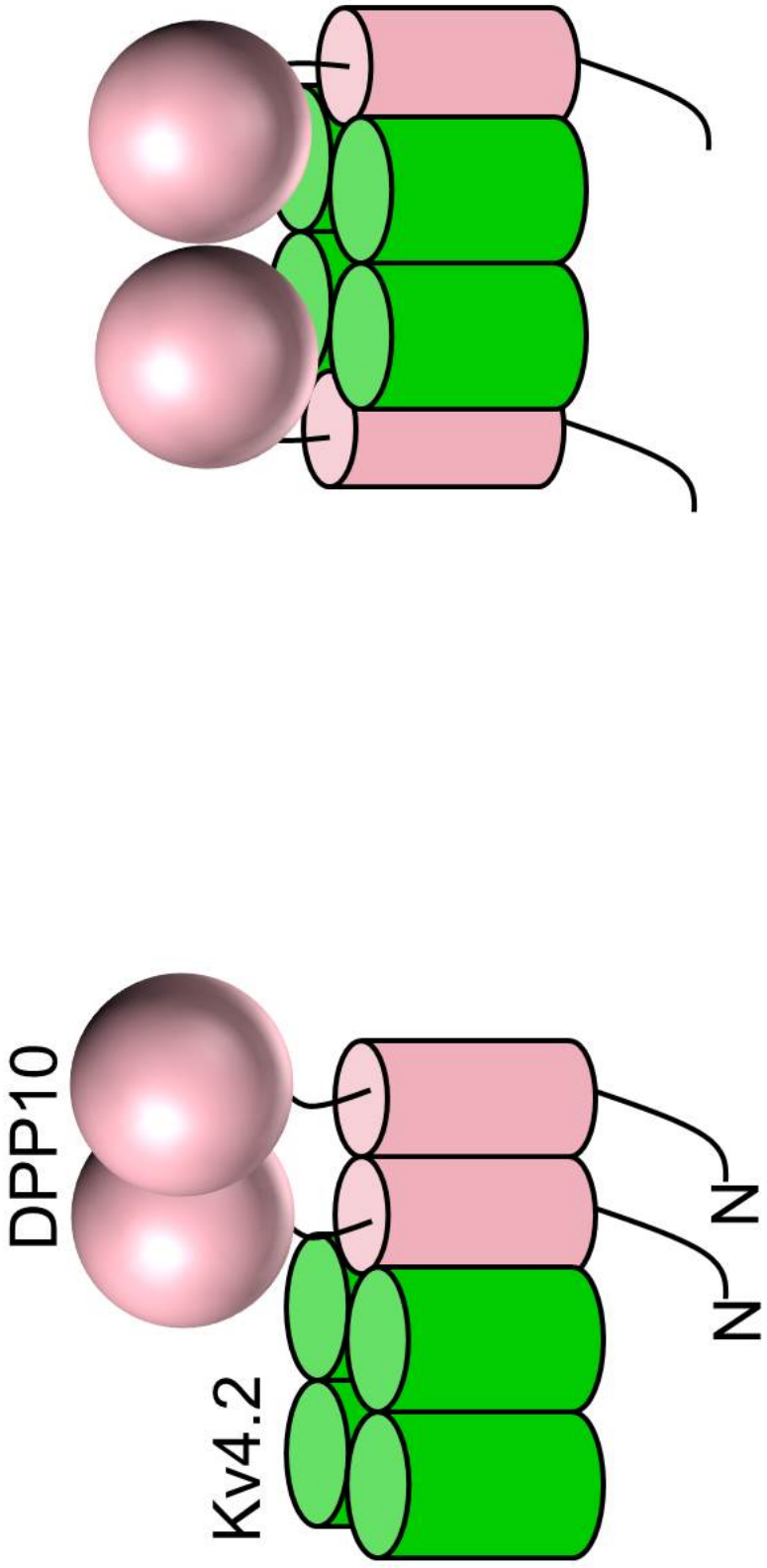

Acknowledgements

I would like to thank Professor Yoshihiro Kubo for his consistent supports and encouragements during the entire course of this doctoral thesis work. I also would like to thank Assistant Professor Koich Nakajo for his continuous supports throughout my 3 years. I would like to thank Dr. Maximilian Ulbrich (Freiburg University) for providing the analysis software for the subunit counting and the vectors for constructing the mEGFP and mCherry fusion proteins. I also would like to thank all members of Kubo laboratory for various discussions, technical advices, encouragements and supports during this work. Finally, I would like to thank my parents for encouraging and supporting me throughout my thesis work.

Parts of this thesis have been published by the authors: Kitazawa, Kubo & Nakajo in Journal of Biological Chemistry (2014). 289:17597-609.